Seismic tomography reveals contrasting styles of subduction-channel and mantle-wedge exhumation controlled by upper plate divergent motion

Stefano Solarino, Marco Malusà, Elena Eva, Anne Paul, Stephane Guillot, Silvia Pondrelli, Simone Salimbeni, Liang Zhao

Gondwana Research 136 (2024) 169–182

Contents lists available at ScienceDirect

Gondwana Research

journal homepage: www.elsevier.com/locate/gr

Seismic tomography reveals contrasting styles of subduction-channel and mantle-wedge exhumation controlled by upper plate divergent motion

Stefano Solarino [a], Marco G. Malusà [b,*], Elena Eva [a], Anne Paul [c], Stéphane Guillot [c], Silvia Pondrelli [d], Simone Salimbeni [d], Liang Zhao [e]

[a] Istituto Nazionale di Geofisica e Vulcanologia, ONT, Genova, Italy
[b] Department of Earth and Environmental Sciences, University of Milano-Bicocca, Milano, Italy
[c] Univ. Grenoble Alpes, Univ. Savoie Mont-Blanc, CNRS, IRD, Univ. Gustave Eiffel, ISTerre, Grenoble, France
[d] Istituto Nazionale di Geofisica e Vulcanologia, sezione di Bologna, Bologna, Italy
[e] Institute of Geology and Geophysics, Chinese Academy of Sciences, Beijing, China

ARTICLE INFO

Article history:
Received 8 March 2024
Revised 13 August 2024
Accepted 20 August 2024
Available online 12 September 2024
Handling Editor: N. Rawlinson

Keywords:
CIFALPS passive seismic experiments
Moho-like interface
Subduction channel
Western Alps
Eastern Papua New Guinea
Dabie Shan

ABSTRACT

In fossil subduction zones associated with massive exhumation of (ultra)high-pressure ((U)HP) rocks such as the Western Alps, the geometry and behavior of subduction-channel and mantle-wedge rocks during exhumation are still poorly constrained by independent geophysical observations. Here we use a new local earthquake tomography model of the entire fossil subduction zone of the Western Alps based on data collected during the CIFALPS and CIFALPS2 passive seismic experiments, and the first receiver-function profile across the Ligurian Alps, to investigate the styles of subduction-channel and mantle-wedge exhumation as a function of increasing upper-plate divergence motion. In the northern Western Alps (low divergence), a thickened subduction channel can be detected, but no exhumed mantle wedge is found beneath the Gran Paradiso (U)HP dome. In the southern Western Alps (intermediate divergence), an exhumed mantle wedge is detected beneath the Dora-Maira (U)HP dome above a serpentinized subduction channel. In the Ligurian Alps (high divergence), an exhumed mantle wedge and a former subduction channel are detected at much shallower levels beneath the Voltri-Valosio (U)HP dome, and above a shallow-dipping lower-plate Moho. In this latter case, the lower boundary of the exhumed subduction channel is the most evident seismic-velocity interface, which may be easily misinterpreted as a true Moho. Similar Moho-like interfaces are found beneath the exhumed (U)HP domes of eastern Papua New Guinea and the Dabie Shan, which suggests that the results of the CIFALPS experiments may be used as a reference case for the interpretation of other (U)HP terranes worldwide.

1. Introduction

Cenozoic subduction zones associated with massive exhumation of (ultra)high-pressure ((U)HP) rocks of continental origin, such as the Western Alps and eastern Papua New Guinea (e.g., Chopin, 1984; Baldwin et al., 2004) are characterized by a component of upper-plate divergent motion that varies along strike (Webb et al., 2008; Baldwin et al., 2012; Malusà et al., 2011; 2015). In these tectonic settings, thermo-mechanical numerical models predict an invariably fast buoyant rise of subducted continental (U)HP rocks, which form tectonic domes exposed at the Earth's surface, and contrasting styles of exhumation of subduction-channel and mantle-wedge rocks depending on the amount of upper-plate divergent motion (Liao et al., 2018). However, unlike the fast exhumation of (U)HP tectonic domes predicted by numerical models, which is confirmed by petrological and geochronological evidence (e.g., Rubatto and Hermann, 2001; Baldwin et al., 2008), the geometry of the subduction channel and the behavior of mantle-wedge rocks during exhumation are still poorly constrained by independent geophysical observations. The Western Alps (Fig. 1) represent a world-reference example of fossil subduction zone, because their subduction wedge is well exposed and the structures related to the (U)HP exhumation stage are exceptionally well preserved (Malusà et al., 2015, 2021) and virtually undeformed since the Oligocene, as attested by the

* Corresponding author.
E-mail address: marco.malusa@unimib.it (M.G. Malusà).

https://doi.org/10.1016/j.gr.2024.08.016
1342-937X/

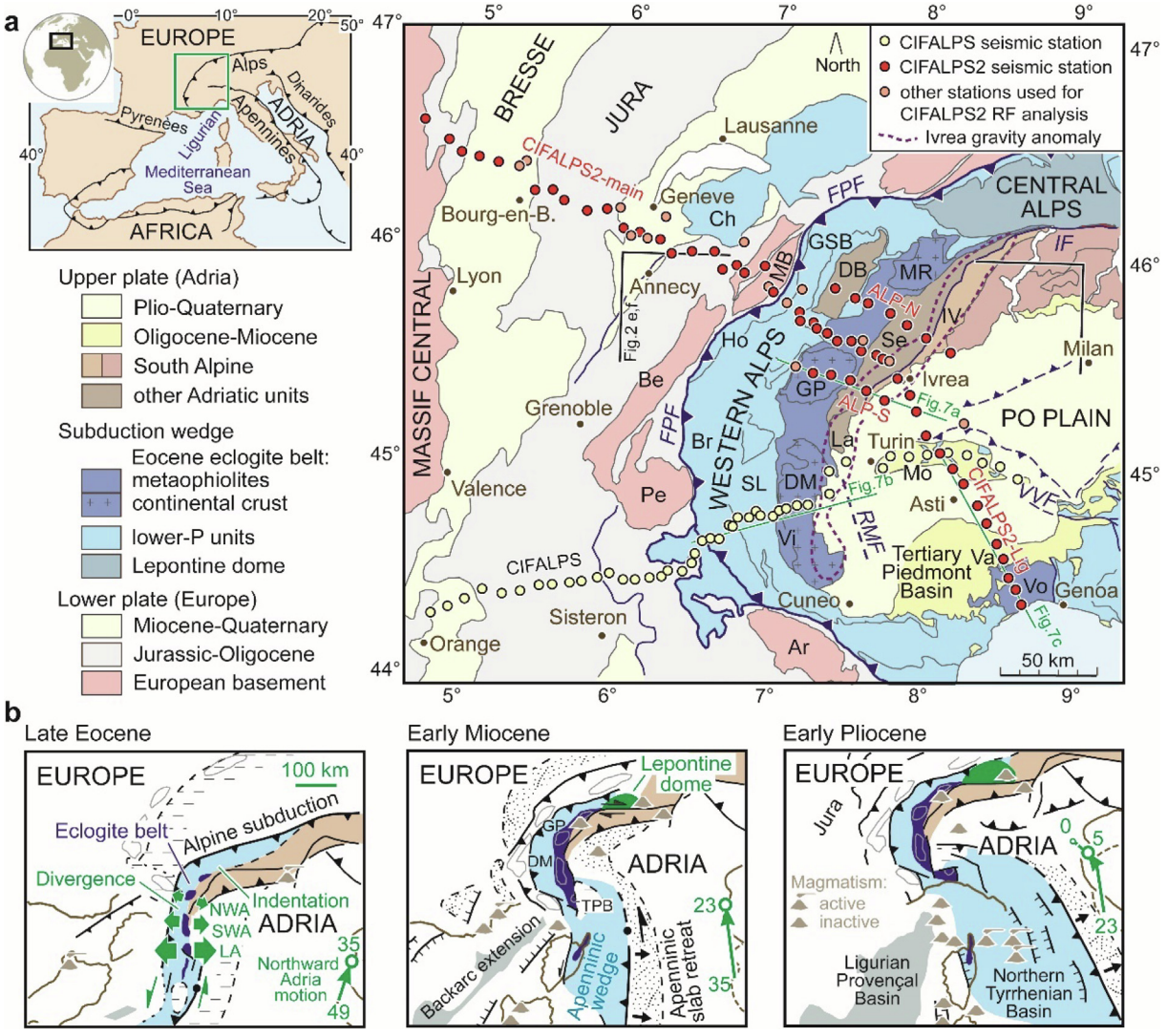

Fig. 1. Tectonic setting of the fossil subduction zone of the Western Alps and locations of the CIFALPS temporary seismic experiments. a: Sketch map of the western Mediterranean and tectonic map of the Western Alps (after Malusà et al., 2021). The red dots indicate the seismic stations of the CIFALPS2 seismic profiles (CIFALPS2-main, CIFALPS2-Lig and complementary ALP-N and ALP-S profiles) (Zhao et al., 2018), the yellow dots mark the seismic stations of the CIFALPS profile (Zhao et al., 2015). The 0-mGal contour of the Ivrea gravity anomaly (purple dashed line, from Zahorec et al., 2021) is also shown. The green lines indicate the interpretive geologic cross sections of Fig. 7. b: Palinspastic reconstruction of the Alpine subduction zone in the Late Eocene (ca. 35 Ma), Early Miocene (ca. 23 Ma), and Early Pliocene (ca. 5 Ma), showing progressive indentation of Adriatic lithosphere in the Central Alps and southward-increasing divergence in the Western Alps during exhumation of the Eclogite belt (dark blue), from the northern Western Alps (NWA) to the southern Western Alps (SWA) and the Ligurian Alps (LA) (after Malusà et al., 2021). Other acronyms: Ar, Argentera; Be, Belledonne; Br, Briançonnais; Ch, Chablais; DB, Dent Blanche; DM, Dora-Maira; FPF, Frontal Pennine Fault; GP, Gran Paradiso; GSB, Grand St-Bernard; Ho, Houiller; IF, Insubric Fault; IV, Ivrea-Verbano; La, Lanzo; MB, Mont Blanc; MR, Monte Rosa; Pe, Pelvoux; RMF, Rivoli-Marene Fault; Se, Sesia-Lanzo; SL, Schistes lustrés; TPB, Tertiary Piedmont Basin; Va, Valosio; Vi, Viso; Vo, Voltri; VVF, Villalvernia-Varzi Fault.

relationships with the overlying Oligocene-Miocene sedimentary rocks of the Tertiary Piedmont Basin (Cassano et al., 1986; Malusà et al., 2015). Some recent studies have analyzed along-strike variations in the deep tectonic structure of the Western Alps (e.g., Nouibat et al., 2022; Nouibat et al., 2023; Paul et al., 2022; Menichelli et al., 2023; Zhao et al., 2020), for example Paul et al. (2022) who used coupled receiver-function and ambient-noise tomography to document a marked change in the dip of European Moho from the northern to the southern Western Alps. However, their analysis was not extended southward to the Ligurian Alps, where extreme upper-plate divergent motion is predicted by geodynamic reconstructions (Malusà et al., 2015; 2021) (Fig. 1b). As a result, potential lateral variations in velocity structure within the fossil subduction zone are not yet sufficiently constrained.

Local earthquake tomography is a suitable method for revealing the velocity structure of the Earth's interior through the analysis of earthquakes that occurred within the investigated volume (Kissling, 1988). A reliable local earthquake tomography requires that the study volume is sampled by a dense distribution of seismic rays, which requires a high-quality seismic dataset and an adequate distribution of both earthquakes and receivers (Solarino, 2024). In this study, we use a new local earthquake tomography model based on data recently collected during the CIFALPS and CIFALPS2 passive seismic experiments (Zhao et al., 2016; 2018) to investigate the style of subduction-channel and mantle-wedge exhumation in the entire fossil subduction zone of the Western Alps, from the northern Western Alps to the Ligurian Alps. The local earthquake tomography model is complemented by the first receiver-function profile across the Ligurian Alps (CIFALPS2-Lig profile). Our results are finally compared with the geophysical information available for eastern Papua New Guinea and the Dabie Shan, demonstrating that the results of the CIFALPS experiments have general validity and can provide a reference case to improve the interpretation of the deep tectonic structure of other (U)HP terranes worldwide.

2. Tectonic setting

The Western Alps formed during Late Cretaceous to Paleogene subduction of the Tethyan oceanic lithosphere and adjacent European paleomargin beneath the Adriatic continental microplate (Handy et al., 2010; Malusà et al., 2015). Metamorphic rocks related to Alpine subduction are exposed between two major faults, the Frontal Pennine Fault on the lower-plate side of the orogen, and the Insubric Fault on the upper-plate side (FPF and IF, respectively, in Fig. 1a), where the strongly positive Ivrea gravity anomaly (e.g., Zahorec et al., 2021) (dashed purple line in Fig. 1a) provides evidence of mantle rocks exhumed to shallow depth beneath the western Po Plain. Rocks derived from the hyperextended Adriatic paleomargin (Se in Fig. 1a) were accreted against the Adriatic upper plate at an early stage of subduction, i.e., in the Late Cretaceous (e.g., Chen et al., 2023) and are juxtaposed to eclogitized mantle rocks of the Lanzo massif (La in Fig. 1a) (Rubatto et al., 2008). Paleogene subduction mainly involved oceanic lithosphere and rocks derived from the European paleomargin, leading to the formation of two main tectonic domains with specific metamorphic imprint (Malusà et al., 2011): (i) the Eocene Eclogite belt (dark blue in Fig. 1a), consisting of (U)HP continental crustal domes (DM, GP, MR and Va in Fig. 1a) tectonically enveloped by (U)HP metaophiolites (Vi and Vo in Fig. 1a) (Rubatto and Hermann, 2001; Starr et al., 2020; Manzotti et al., 2022; Ghignone et al., 2023); and (ii) a doubly-vergent frontal wedge of lower-pressure units of oceanic (SL) and European derivation (Br and GSB, light blue in Fig. 1a) (Malusà et al., 2005; Dumont et al., 2022). Rocks exposed in the Eclogite belt were buried in the Alpine subduction channel to be rapidly exhumed to the Earth's surface at rates of 1–3 cm/yr between ~35 Ma and 32 Ma. Rapid exhumation was triggered by episodic upper-plate divergent motion that provided sufficient space for exhumation without requiring overburden removal by erosion (Malusà et al., 2015; Liao et al., 2018). Notably, a southward increase in divergence affected the Western Alps trench in the Eocene, which was a direct consequence of coeval indentation of Adriatic lithosphere beneath the future Central Alps in the north (Fig. 1b) (Malusà et al., 2015; Solarino et al., 2018). The strongest divergence was thus experienced by the segment of Alpine subduction zone now exposed in the Ligurian Alps. This latter region also experienced major counterclockwise fault-block rotations during the Neogene opening of the Ligurian-Provençal basin and the northward propagation of Apenninic tectonics (Fig. 1b), which led to the formation of the Villalvernia-Varzi-Ottone strike-slip fault (VVF in Fig. 1a), the Monferrato thrust fronts (Mo in Fig. 1a), and the Rivoli-Marene Fault (RMF in Fig. 1a) in the western Po Plain (Maffione et al., 2008; Malusà and Balestrieri, 2012; Eva et al., 2020; 2023).

Thermo-mechanical numerical models of (U)HP rock exhumation suggest that major upper-plate divergent motion may also trigger exhumation of subduction-channel and mantle-wedge rocks at depth (Liao et al., 2018). In the Western Alps, evidence for mantle-wedge rocks exhumed to shallow depths was first reported beneath the Dora-Maira (U)HP dome by Solarino et al. (2018), and stacked remnants of a fossilized serpentinite channel were first imaged at depth around 60 km by Zhao et al. (2020) along the CIFALPS profile.

3. Data and methods

The CIFALPS2 passive seismic experiment (Zhao et al., 2018) was designed as a complement to the CIFALPS project recently performed across the southern Western Alps (Zhao et al., 2015, 2016; Malusà et al., 2021) (Fig. 1a). Fifty-six broadband seismic stations were installed with a spacing of 7–10 km from the Bresse Graben to the Ligurian Sea. The trend of the main profile is WNW-ESE across the northern Western Alps (CIFALPS2-main profile in Fig. 1a) and NNW-SSE across the Ligurian Alps (CIFALPS2-Lig in Fig. 1a), with a main change in direction near the town of Ivrea in the western Po Plain. Two complementary profiles (ALP-N and ALP-S in Fig. 1a) were also deployed across the internal part of the northern Western Alps and the Eocene eclogite belt, parallel to the CIFALPS2-main profile. Seismic stations were equipped with broadband sensors and connected by Global System for Mobile communications for real time data acquisition. This allowed us to remotely check the instrument state-of-health and intervene promptly to avoid data losses. Stations were in operation from fall 2018 to winter 2019, but a few stations in the northern Western Alps were already installed in June 2018 and operated until June 2020.

To perform local earthquake tomography, data collected during the CIFALPS and CIFALPS2 experiments were merged with those recorded by permanent seismic networks operating in Italy, France, and Switzerland and available from the EIDA database (Fig. 2a). This allowed us to expand the study area and improve the cross-firing of seismic rays at each node of the model (Fig. 2b). We did not use data recorded by the temporary seismic network AlpArray (Hetényi et al., 2018), which was operational in almost the same period and more widely spaced, because most of the stations of that project were located in areas where we already had a good ray coverage due to both permanent and CIFALPS and CIFALPS2 temporary stations. The maximum depth of investigation of a local earthquake tomography depends on the deepest events available for analysis in the study volume. Because intermediate-depth earthquakes are not frequent in the western Alpine region, only a few of these events were recorded during the CIFALPS and CIFALPS2 experiments. The dataset was thus integrated with intermediate-depth earthquakes (Eva et al., 2015; Malusà et al., 2017) from available seismic catalogs (https://www.orfeus-eu.org/data/eida/) to ensure an adequate sampling of the bottom part of the model (Fig. 2c). A similar integration was performed at the corners of the model to cope with areas where few earthquakes occurred or where no station was installed. As a result, the initial database consisted of about 2000 seismic events. All events were hand picked and show an uncertainty ranging from 0.01 to 0.2 s depending on the phase and weight attributed to the pick. Because the initial distribution of seismic events was not optimal for seismic tomography, we used a software code designed to evenly distribute the events and avoid redundant information and overconcentration of rays in specific sectors of the modelled volume. As a first step, data not compliant with quality criteria (less than 10P+S phase readings, location outside the study volume) were discarded from the database. As a second step, the study volume was subdivided into cells with 5-km spacing. A maximum number of 10 events was allowed for each cell. Whenever a single cell included more than 10 events, a selection was made by the algorithm based on the number of phase picks. The number of P readings for each station is shown in the 3-D histogram of Fig. 2d, whereas the three-dimensional P ray coverage is shown in Fig. 2b. We used as input 1420 events, 6700P and 5745 S picks.

Local earthquake tomography was carried out using SIMULPS14, a version of SIMULPS (Thurber, 1983; Eberhart-Phillips, 1990) incorporating full 3-D ray shooting (Haslinger & Kissling 2001). The grid consists of $38\times38\times13$ nodes, with spacing of 10 km in the central part of the model and 20 km elsewhere, whereas in the extremes of the model spacing is 30 km. Damping was optimized by plotting trade off model/data variance curves. The initial root-mean-square residual was 0.96364 and the data variance 0.125905. After tomographic inversion, root-mean-square residual dropped to 0.78779 and the variance to 0.068342.

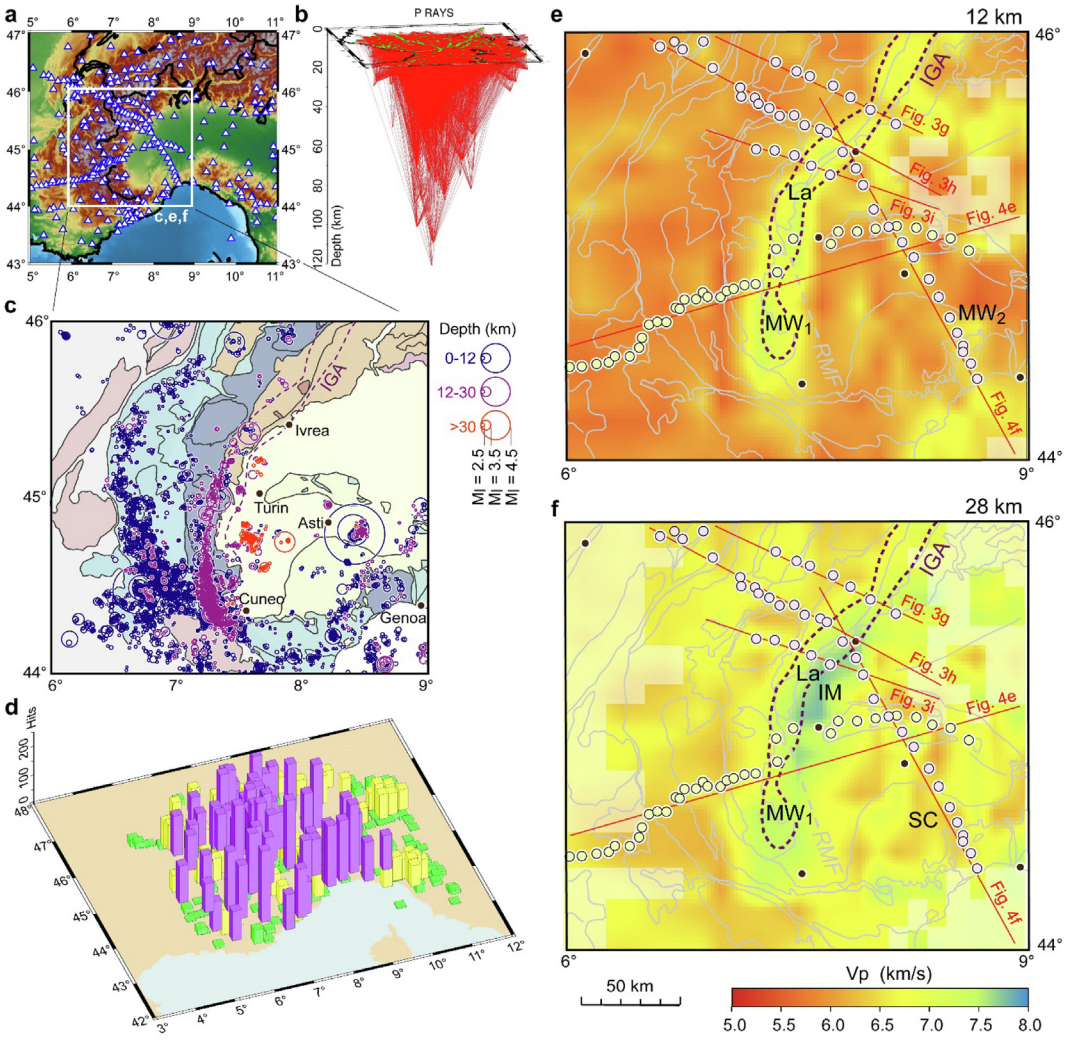

Fig. 2. Local earthquake tomography set up and Vp depth slices. a: Distribution of seismic stations (triangles) considered for local earthquake tomography. b: three-dimensional P ray coverage. c: Depth distribution of HypoDD-relocated seismic events, geological map as in Fig. 1a (after Eva et al., 2020). d: 3-D histogram showing the number of P readings for each station (green: <50; yellow: 50–100; purple: >100). e-f: Depth slices of the Vp tomography model at 12 and 28 km depth. The main geological boundaries (grey), the Ivrea gravity anomaly (IGA) and the CIFALPS seismic stations (big dots) are shown for reference. Areas not resolved (resolution of diagonal elements < 0.1) are masked. The red lines indicate the Vp cross sections of Figs. 3 and 4. Acronyms: IM=Ivrea mantle; La = Lanzo peridotite; MW_1, MW_2 = exhumed mantle-wedge; SC=subduction channel.

The reliability of the structural images delineated by local earthquake tomography is validated by synthetic tests (see Supplementary material) and by a comparison with the seismic images provided by receiver function (this work and Paul et al., 2022) and ambient-noise tomography (Nouibat et al., 2022). We consider the comparison between these three totally independent methods, which analyze different seismic events using different processing techniques, as a better proof of reliability than any other type of test. Indeed, local earthquake tomography is based on the analysis of earthquakes within the model volume, while ambient-noise tomography images the S-wave velocity structure in the crust and uppermost mantle based on noise cross-correlations, and receiver function exploits teleseismic events and P-to-S (Ps) converted waves at velocity interfaces beneath seismic stations (Langston, 1979). A strength of the receiver function analysis is that it allows detection of interfaces with downward velocity increase, for example the Moho, and interfaces with downward velocity decrease because the polarity of the converted signal depends on the sign of the velocity change (see, e.g., Zhao et al., 2015). For the CIFALPS2-Lig profile, we used the same approach to receiver function analysis described in Paul et al. (2022), including multichannel preprocessing (Rondenay, 2009; Millet et al., 2019) to attenuate the direct P wave and enhance the converted phases from shallow interfaces, and time-to-depth common-conversion point migration using 2-D sections in the ambient-noise tomography model by Nouibat et al. (2022) as crustal velocity models.

4. Results

Fig. 2e-f show two Vp horizontal slices of the local earthquake tomography model at 12 and 28 km depth, where areas not resolved are masked. Figs. 3 and 4 show five vertical cross-sections of the local earthquake tomography model across the northern Western Alps, the southern Western Alps, and the Ligurian Alps, which are compared with seismic images provided by receiver function and ambient-noise tomography along the same profiles. Only those interfaces independently detected by at least two different methods are indicated and labeled in the cross-sections for further discussion in the text. As shown in Fig. 2e-f, the Alpine fossil subduction zone is well resolved from the northern Western Alps to the Ligurian Alps. Low resolutions characterize

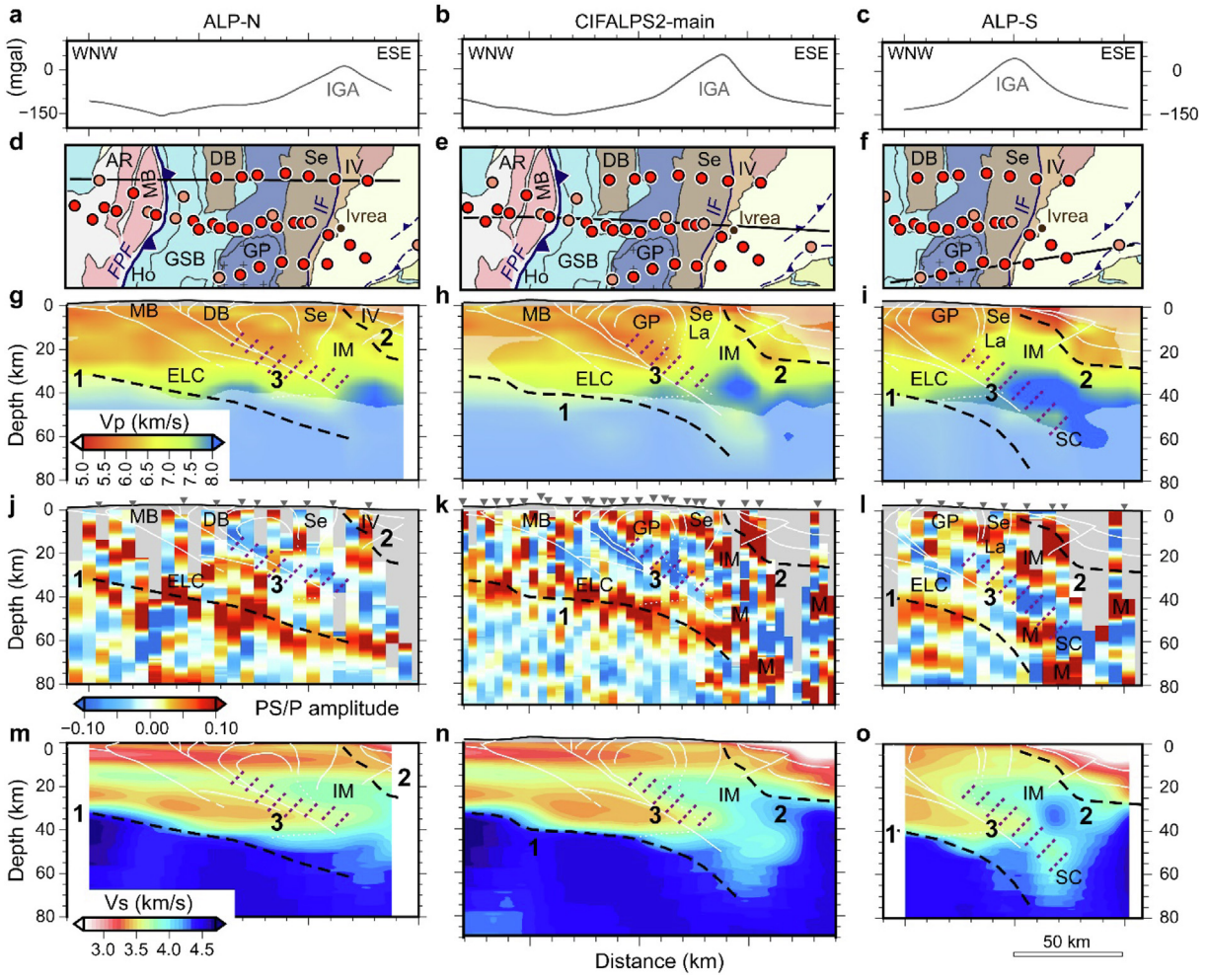

Fig. 3. Depth sections across the northern Western Alps (left column: ALP-N profile; central column: CIFALPS2-main profile; right column: ALP-S profile). a-c: Bouguer anomaly from the gravity database of Zahorec et al. (2021) (IGA=Ivrea gravity anomaly). d-f: Geological maps with profile locations (black lines). g-i: P-wave velocity structure from local earthquake tomography (this work). j-l: Common-conversion-point stacked section for teleseismic earthquakes of 0-100° back-azimuth (redrawn after Paul et al., 2022). m-o: Vs section from the ambient-noise tomography model of Nouibat et al. (2022). Note the consistency between interfaces identified by the three independent imaging methods. The dashed black lines mark interfaces with a downward velocity increase (1 = European Moho; 2 = Adriatic Moho), whereas the dotted purple boundaries (3) mark interfaces with a downward velocity decrease. ELC=European lower crust; M=multiples; other acronyms as in Fig. 1a and 2e, f. See locations in Fig. 1a and 2.

instead the western Po Plain to the north of the Monferrato thrust fronts and, in the 28-km depth slice, the Ligurian Sea and the Belledonne and Pelvoux massifs (Be and Pe in Fig. 1a), which represent lower-plate units not involved in the subduction wedge. In the 12-km depth slice, the Ivrea gravity anomaly corresponds to a region with high P-wave velocities (yellow-to-green in Fig. 2e), which also includes the exposure area of the eclogitized mantle rocks of the Lanzo massif and the mantle-wedge rocks exhumed to shallow depth beneath the Dora-Maira (U)HP dome (Solarino et al., 2018) (La and MW_1, respectively, in Fig. 2e). In the same region, the seismic velocity fingerprint of the Ivrea mantle (IM in Fig. 2f) becomes clearly distinguishable in the 28-km depth slice, where it shows Vp >7.7 km/s. In the Ligurian Alps, along the CIFALPS2-Lig profile, high Vp values ~6.5 km/s are found in the 12-km depth slice (MW_2 in Fig. 2e) and are replaced by lower Vp values ~6.0 km/s in the 28-km depth slice (SC in Fig. 2f).

4.1. CIFALPS2-main profile and ALP-N and ALP-S complementary profiles

In the northern Western Alps, the local earthquake tomography model reveals the P-wave velocity structure in the region above the European Moho down to 40–45 km depth along the ALPS-N and CIFALPS2-main profiles, and down to 65 km depth along the ALP-S profile (Fig. 3). The European Moho (labelled "1″), which lays below the area resolved by the local earthquake tomography model, is marked by laterally continuous P-to-S (Ps) converted phases of positive polarity and strong amplitude in the receiver function stacks (Fig. 3j-l), and by the 4.3 km/s S-wave velocity contour in the ambient-noise tomography model (Fig. 3m-o). The Moho dips gently from ~30-km depth beneath the Mont Blanc massif (MB in Fig. 3) to ~45-km depth beneath the Gran Paradiso dome (GP in Fig. 3), reaching 60–70 km depth beneath the western tip of the Adriatic upper plate. A progressive seismic velocity increase is observed in the European lower crust (ELC) starting from 35 to 40 km depth, both in the ambient-noise tomography model and in the local earthquake tomography model, where P-wave velocity reaches ~7.7 km/s at ~40 km depth (Fig. 3g-i). As a result, at depth >40 km, the Ps converted phases are weaker in the receiver function images, as indicated by the orange colors in Fig. 3j-l.

The Adriatic Moho (labelled "2″) is best resolved in the local earthquake tomography model (Fig. 3g-i) compared to the receiver function stack and the ambient-noise tomography model. This is

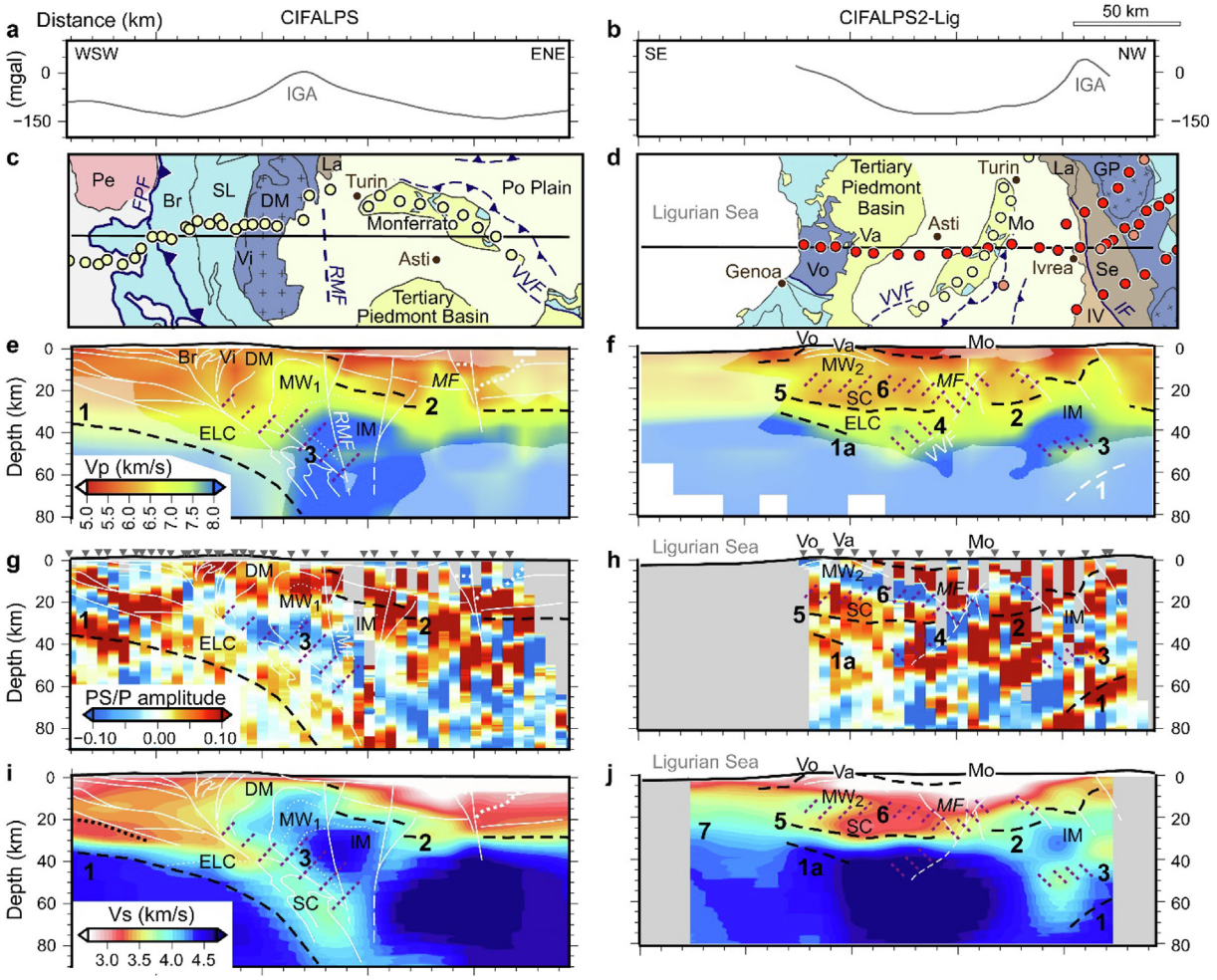

Fig. 4. Depth sections along the southern Western Alps and the Ligurian Alps (left column: CIFALPS profile; right column: CIFALPS2-Lig profile). a-b: Bouguer anomaly from the gravity database of Zahorec et al. (2021) (IGA=Ivrea gravity anomaly). c-d: Geological maps with profile locations (black lines). e-f: P-wave velocity structure from local earthquake tomography (this work). g-h: Common-conversion-point stacked section for teleseismic earthquakes: g = after Paul et al. (2022); h = this work. i-j: Vs section from the ambient-noise tomography model of Nouibat et al. (2022). As in Fig. 3, note the consistency between interfaces identified by the three independent methods. The dashed black lines mark interfaces with a downward velocity increase, whereas the dotted purple boundaries mark interfaces with a downward velocity decrease. ELC=European lower crust; MF=Monferrato flower structure; 1 and 1a = European Moho; 2 = Adriatic Moho; 7 = Ligurian Moho; 3–6 = other seismic interfaces; other acronyms and locations as in Fig. 1a and 2e, f.

due to the low signal-to-noise ratios in the poorly consolidated sediments of the Po Plain that preclude a reliable analysis of Ps conversions (Paul et al., 2022), and to the low horizontal resolution of the ambient-noise tomography model of Nouibat et al. (2022) in the uppermost 10–15 km, as revealed by the numerous near-horizontal Vs interfaces that intersect dipping tectonic boundaries within the subduction wedge as independently constrained by field geology observations and published geological maps (Fig. 3-m-o).

No high-Vp region is observed in the local earthquake tomography model beneath the Gran Paradiso dome, either in the ALP-N, CIFALPS2-main or ALP-S profiles. Along the ALP-N profile, regions with high Vp>7.0 km/s at shallow depth (>12 km) are exclusively to the east of the Insubric Fault (IM in Fig. 3g). Along the CIFALPS2-main and ALP-S profiles, regions with high Vp>7.0 km/s are also found beneath the Sesia-Lanzo unit to the west of the Insubric Fault, where they likely mark the Lanzo mantle slivers (Fig. 3h-i). A low-Vp spot is observed in the lower part of the local earthquake tomography model at ~50 km depth along the ALP-S profile (SC in Fig. 3i), right in the place where a low-Vs spot is observed in the ambient-noise tomography model (Fig. 3o), and where a set of diffuse negative-polarity Ps converted phases (labelled "3″) is observed in-between the Adriatic and the European Mohos (Fig. 3l). In a recent methodological study, Virieux et al. (2024) tested the reliability of local earthquake tomography for crustal imaging by using the Western Alps as a case study. They concluded that the earthquake distribution allows a reconstruction of robust features down to 40-km depth whatever the tomography strategy and parameters, but the poor resolution of the local earthquake tomography model comparisons at > 40 km depths would preclude a reliable imaging of the deepening of the European Moho beneath the Western Alps (Virieux et al., 2024). This would suggest that the low-Vp spot labelled SC in Fig. 3i may be not robust. However, a similar anomaly is independently imaged by ambient-noise tomography (Fig. 3o), which underlines the importance of comparing seismic images based on independent methods for a better proof of reliability.

4.2. CIFALPS profile

In the southern Western Alps, the new local earthquake tomography model (Fig. 4e) confirms the main features highlighted by Solarino et al. (2018), Nouibat et al. (2022), Paul et al. (2022) and Virieux et al. (2024). The European Moho (labelled "1″) is marked

by laterally continuous Ps converted phases of positive polarity and strong amplitude in the receiver function stacks (Fig. 4g), and by the 4.3 km/s S-wave velocity contour in the ambient-noise tomography model (Fig. 4i). It dips from ~40 km depth beneath the Frontal Pennine Fault (FPF in Fig. 4c) to ~60 km depth beneath the Dora-Maira dome (DM in Fig. 4), reaching 85–90 km depth beneath the western tip of the Adriatic upper plate and the Rivoli-Marene Fault (RMF in Fig. 4). Like in the northern Western Alps, the amplitude of the Ps conversions decreases starting from 35 to 40 km depth, due to an increase in seismic velocity in the European lower crust (ELC in Fig. 4) that is visible in both Vp and Vs models (Fig. 4e, 4i). The Adriatic Moho (labelled "2") is well resolved in the local earthquake and ambient-noise tomography models, and it is cut by lithospheric faults that bound a high-Vp region (up to 7.5 km/s, MF in Fig. 4e) located near the town of Asti. In the western part of the profile, the uppermost part of the Alpine subduction wedge shows Vp values invariably <6.5 km/s (Fig. 4e), but a prominent high velocity body (Vp ~7–7.5 km/s) is imaged beneath the Dora-Maira (U)HP dome, at depths from ~10 km to >30 km. This high velocity body (MW_1 in Fig. 4e), which was already interpreted as an exhumed mantle wedge by Solarino et al. (2018) and Malusà et al. (2021), is also evident in the ambient-noise tomography model of Nouibat et al. (2022), but with a slightly different shape which may be either due to horizontal smearing affecting the uppermost part of the ambient-noise tomography model, as described in Sect. 4.1, or to the presence of rocks with lower Vp and higher Vs to the west of MW_1. The high seismic velocities of the exhumed mantle wedge contrast with the low seismic velocities detected in the underlying subduction channel (Vs <3.7 km/s according to Zhao et al., 2020; Vs ~3.8 km/s according to Nouibat et al., 2022) which produces an evident set of negative-polarity Ps phases (labelled "3") in the receiver function stacks.

4.3. CIFALPS2-Lig profile

The southern part of the CIFALPS2-Lig profile, south of the Monferrato thrust front, provides a further, unexplored cross-section of the Alpine subduction wedge (Fig. 4b, d, f, h, j). Along this cross section, the European foreland was originally located in the position of the current Ligurian-Provençal basin (Ligurian Sea in Fig. 4d), which formed in the Miocene during the rollback of the Apenninic slab, the northward propagation of Apenninic tectonics and the consequent formation of the Monferrato thrust fronts (Mo in Fig. 4d). The velocity structure of the Ligurian-Provençal basin is nicely imaged by ambient-noise tomography (Fig. 4j), and it is strikingly different from the velocity structure that is observed onshore beneath the Ligurian Alps, because it is much younger and unrelated to Alpine subduction. In the northern part of the CIFALPS2-Lig profile, to the north of the Monferrato thrust front, the seismic images show the same deep structure already described for the northern Western Alps (cf. Fig. 3), with a SE-dipping European Moho (labelled "1″) that is separated from the overlying Adriatic Moho (labelled "2") by an interface of downward decreasing seismic velocities that produce a set of diffuse negative-polarity Ps converted phases (labelled "3") (Fig. 4f, h). Along the receiver function profile, the Monferrato thrust front is marked by a south-dipping set of diffuse negative-polarity Ps converted phases cutting across the entire crust (labelled "4" in Fig. 4h).

The European Moho under the Ligurian Alps (labelled "1a") is detected by local earthquake tomography beneath the Eocene eclogite belt (Vo and Va in Fig. 4), where it dips gently northward from ~30 km depth, near the coastline, to ~40 km depth beneath the tip of the Tertiary Piedmont Basin (Fig. 4f), and it is also consistently imaged by receiver function (Fig. 4h) and ambient-noise tomography (Fig. 4j). In the ambient-noise tomography model of Nouibat et al. (2022), the interface labelled "1a" (Fig. 4j) corresponds to the same S-wave velocity contour of 4.3 km/s that marks the European Moho in the Western Alps (Fig. 3n, 4i), and it is also marked by weak positive-polarity Ps converted phases in the receiver function stacks (Fig. 4h). Above the European Moho labelled "1a" there are laterally continuous Ps converted phases of positive polarity and strong amplitude that are observed in the receiver function stacks at ~25–30 km depth, marking an interface (labelled "5") with a sharp downward increase in seismic velocities (Fig. 4h). This velocity change is clear in the local earthquake tomography model, where Vp values ~6.0 km/s at 20–30 km depth, above interface 5 (SC in Fig. 4f), are replaced below the same interface by Vp values of ~7.0–7.5 km/s typical of the European lower crust (ELC in Fig. 4f). These latter Vp values progressively increase from ~7.0 km/s to ~7.5 km/s moving northward and at constant depth towards the Monferrato thrust front. A sharp change in seismic velocities across interface 5 is also observed in the ambient-noise tomography model (Fig. 4j), where Vs values are as low as 3.0 km/s above interface 5 and ~4.0 km/s below it. A further set of laterally continuous Ps converted phases of negative polarity and strong amplitude, labelled "6" and gently dipping to the north, is observed at ~20 km depth beneath the Eocene eclogite belt and the Tertiary Piedmont Basin (Fig. 4h). In the local earthquake tomography model, interface 6 separates the region with low Vp values ~6.0 km/s located at 20–30 km depth (SC in Fig. 4f) from an overlying region of higher Vp ~6.5 km/s located right beneath the Voltri and Valosio units (MW_2 in Fig. 4f). In the ambient-noise tomography model, interface 6 separates a region with Vs values as low as 3.0 km/s from an overlying region with Vs ~ 3.7 km/s (Fig. 4j).

5. Discussion

5.1. Styles of subduction-channel and mantle-wedge exhumation

The local earthquake tomography and receiver function analyses performed along the CIFALPS2-Lig profile complement the already published CIFALPS and CIFALPS2-main results (Malusà et al., 2021; Paul et al., 2022) to provide an unprecedented image of the variable styles of subduction-channel and mantle-wedge exhumation in the Alpine fossil subduction zone as a function of the amount of upper-plate divergent motion along the plate boundary.

A comparison between the vertical cross-sections of Figs. 3 and 4 and the 2-D thermo-mechanical model evolution of Fig. 5, which investigates the exhumation of (U)HP rocks triggered by the divergent motion of the upper plate (Liao et al., 2018), allows to evaluate the amount of divergence during exhumation in the northern Western Alps (~30 km), southern Western Alps (~60 km), and Ligurian Alps (~100 km), consistent with previous geodynamic reconstructions of the Adria-Europe plate-boundary zone (Malusà et al., 2015). The strongest divergence involved segments of the Alpine subduction zone located farther away from the site of coeval Adria indentation beneath the Central Alps (e.g., Malusà et al., 2016) (Fig. 1b). According to this kinematic configuration, divergence in the Ligurian Alps was probably faster, but not more prolonged, than in the northern Western Alps. Note that the modelled size of exhumed (U)HP domes is invariant for different rates of upper plate divergent motion (Liao et al., 2018), while larger amounts of divergence is expected to trigger exhumation of the mantle wedge beneath the exhumed (U)HP domes, with a much larger impact on the deep tectonic structure of the fossil subduction zone. Predicted seismic velocities and resulting interpretive geologic cross sections are shown in Figs. 6 and 7.

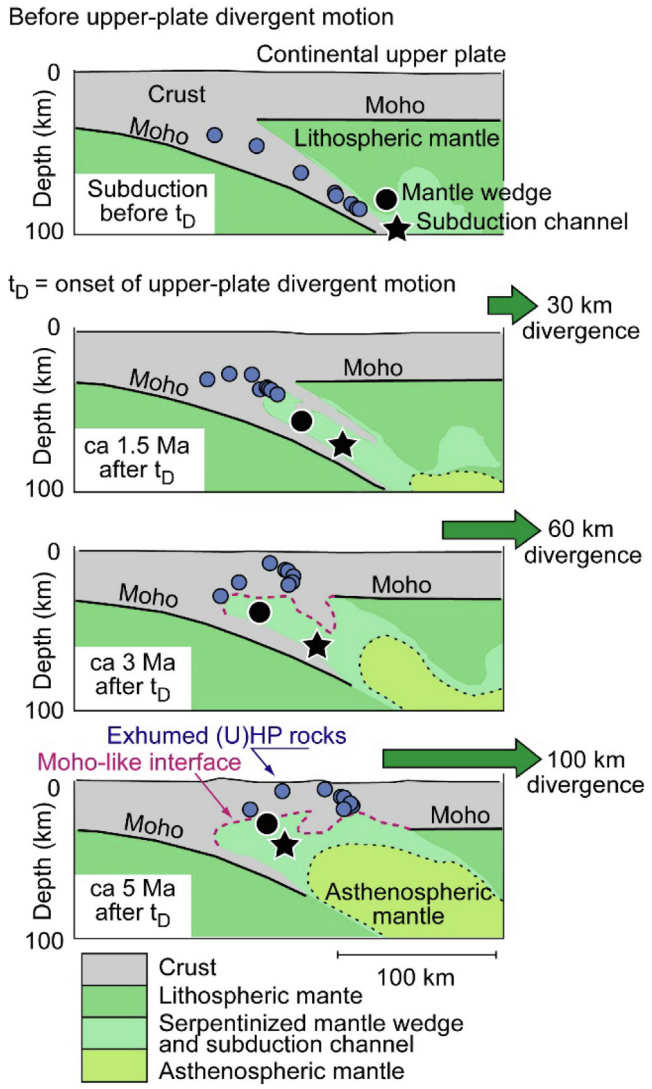

Fig. 5. Modeled relationships between continental (U)HP rocks (blue dots) and mantle rocks (green) during exhumation triggered by upper-plate divergent motion (based on the thermo-mechanical numerical models of Liao et al., 2018). The green arrows are proportional to the divergent motion. The continuous black lines indicate the Moho. The black star marks exhumed rocks of the former subduction channel, the black dot marks rocks of the exhumed mantle wedge. A Moho-like interface (in magenta) may form beneath the exhumed (U)HP tectonic domes where crustal rocks lay directly above mantle rocks after exhumation.

In the northern Western Alps, where the amount of upper-plate divergent motion during exhumation is evaluated at ~30 km (e.g., Liao et al., 2018), the high-Vp regions >7.0 km/s observed beneath the Sesia-Lanzo unit likely mark the eclogitized mantle rocks of the Lanzo massif (La in Fig. 7a). However, no high-Vp body reflecting an exhumed mantle wedge is observed in the local earthquake tomography model beneath the Gran Paradiso (U)HP dome, nor in the ALP-N profile, nor in the CIFALPS2-main or ALP-S profiles. The Adriatic mantle exhumed to the east of the Insubric Fault was exhumed much earlier and represents the necking zone of the Alpine Tethys, as attested by the overlying and almost undeformed Mesozoic sedimentary successions (Berra et al., 2009). Paul et al. (2022) first documented in the northern Western Alps the transition from a shallow-dipping European Moho, detected along the ALP-N and CIFALPS2-main profiles, to a much steeper European Moho detected along the ALP-S profile as well as the CIFALPS profile farther south. Along the ALP-S profile, a low-Vs region (~3.7 km/s) consistent with the occurrence of serpentinite (large black star in Fig. 6) is detected at 50 km depth, which is interpreted as seismic evidence of a thickened subduction channel (black star in Fig. 7a) similarly to what was first proposed by Zhao et al. (2020) for the CIFALPS profile. No seismic evidence of a thickened subduction channel is found farther north, where the European Moho is shallow dipping.

In the southern Western Alps, where the amount of upper-plate divergent motion during exhumation is evaluated at ~60 km (Liao et al., 2018), a prominent high velocity body (Vp ~7–7.5 km/s) is imaged beneath the Dora-Maira (U)HP dome, at depths from ~10 km to >30 km (large black dot in Figs. 6 and 7b). The observed Vp values are consistent with the interpretation of Solarino et al. (2018), who interpreted this body as an exhumed mantle wedge with a degree of serpentinization around 25–50% or even higher. To the west of the exhumed mantle, increasing seismic velocities with depth are observed in the subduction wedge down to 50 km depth, which is consistent with a progressive transformation of metapelites and gneisses that are exposed at the Earth's surface in the Dora-Maira (U)HP dome. However, a S-wave velocity decrease to ~3.7 km/s is observed at depths >50 km along the plate interface (large black star in Figs. 6 and 7b), which is inconsistent with metamorphic phase changes in metapelites and gneisses. The only rock characterized by similar Vs values at depths >50 km is serpentinite, which suggests that this low-velocity anomaly marks a weak serpentinite channel, as already suggested by Zhao et al. (2020). In summary, seismic velocities characterizing an exhumed mantle wedge beneath the southern Western Alps (large black dot in Fig. 7b) are replaced downwards by lower seismic velocities typical of a serpentinized subduction channel and a metasomatized mantle (black star in Fig. 7b), and even deeper by high seismic velocities typical of the European lower crust (ELC in Fig. 7b) and of the lithospheric-mantle peridotite.

In the Ligurian Alps, where the amount of upper-plate divergent motion during exhumation is evaluated at ~100 km (see Fig. 1b and 5), the European Moho is shallow dipping and located at ~40 km depth beneath the Voltri-Valosio (U)HP dome (Fig. 7c). Based on available seismic tomography constraints, the transition with the much deeper and steeply dipping European Moho of the southern Western Alps, located at ~60 km depth beneath the Dora-Maira (U)HP dome (Fig. 7b), may occur at the level of the Rivoli-Marene Fault (RMF in Fig. 2e, f). Like in the southern Western Alps, a region of higher seismic velocities exists in the Ligurian Alps (Vp ~6.5 km/s; Vs ~3.7 km/s) right beneath the Eocene eclogite belt, which is replaced downward by a region of lower seismic velocities (Vp ~6.0 km/s; Vs ~3.0–3.1 km/s) that lies above the European lower crust (Vp ~7.0–7.5 km/s) (ELC in Fig. 4f). This transition, which occurs in a depth interval of 70–80 km in the case of the southern Western Alps (Fig. 7b), is completed in a depth interval of only 35–40 km in the Ligurian Alps (Fig. 7c). By analogy with the southern Western Alps, we interpret the region of higher seismic velocity beneath the Voltri-Valosio (U)HP dome as an exhumed mantle wedge (MW_2 in Fig. 4f; black dot in Fig. 7c), and the region of lower seismic velocity that lies above the European lower crust as an exhumed subduction channel (SC in Fig. 4f; black star in Fig. 7c). However, seismic velocities are lower in the exhumed mantle wedge and the subduction channel beneath the Ligurian Alps than in the corresponding regions of the southern Western Alps. In fact, after upper-plate divergent motion, protracted residence of these rocks at shallow depths under greenschist-facies conditions possibly led to additional serpentinization of the exhumed mantle wedge, and transformation of high-temperature serpentinite of the exhumed subduction channel into low-temperature serpentinite (small black dot and small star, respectively, in Fig. 6), with consequent reduction in their seismic velocities.

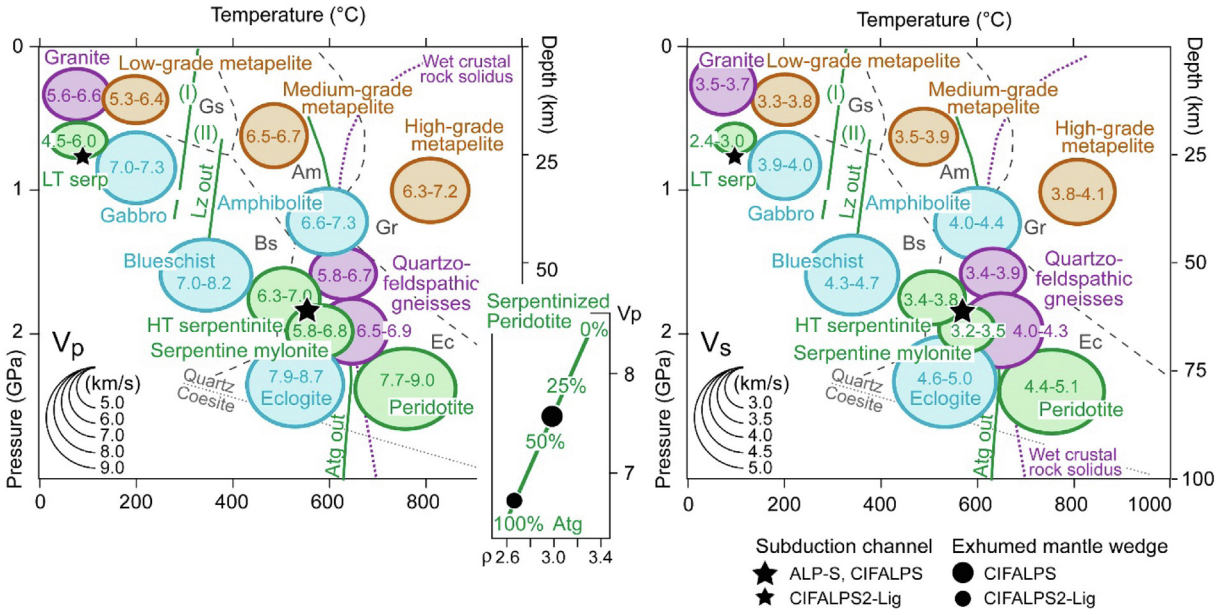

Fig. 6. Seismic velocities in the subduction channel and exhumed mantle wedge along the CIFALPS profiles compared to laboratory-measured seismic velocities (after Malusà et al., 2021 and references therein). The size of the ellipses is proportional to the maximum and minimum seismic velocities; ellipse location depends on the pressure–temperature range at equilibrium for each rock type (green = ultramafic; blue = mafic; purple = granitic; brown = pelitic). Seismic velocities in the subduction channel (black stars) and exhumed mantle wedge (black dots) invariably point to ultramafic rocks, despite Vp and Vs systematically increasing with depth and metamorphic grade. Metamorphic facies acronyms: Am = Amphibolite; Bs = Blueschist; Ec = Eclogite; Gr = Granulite; Gs = Greenschist. Wet crustal-rock solidus for granitic rocks after Schmidt et al. (2004).

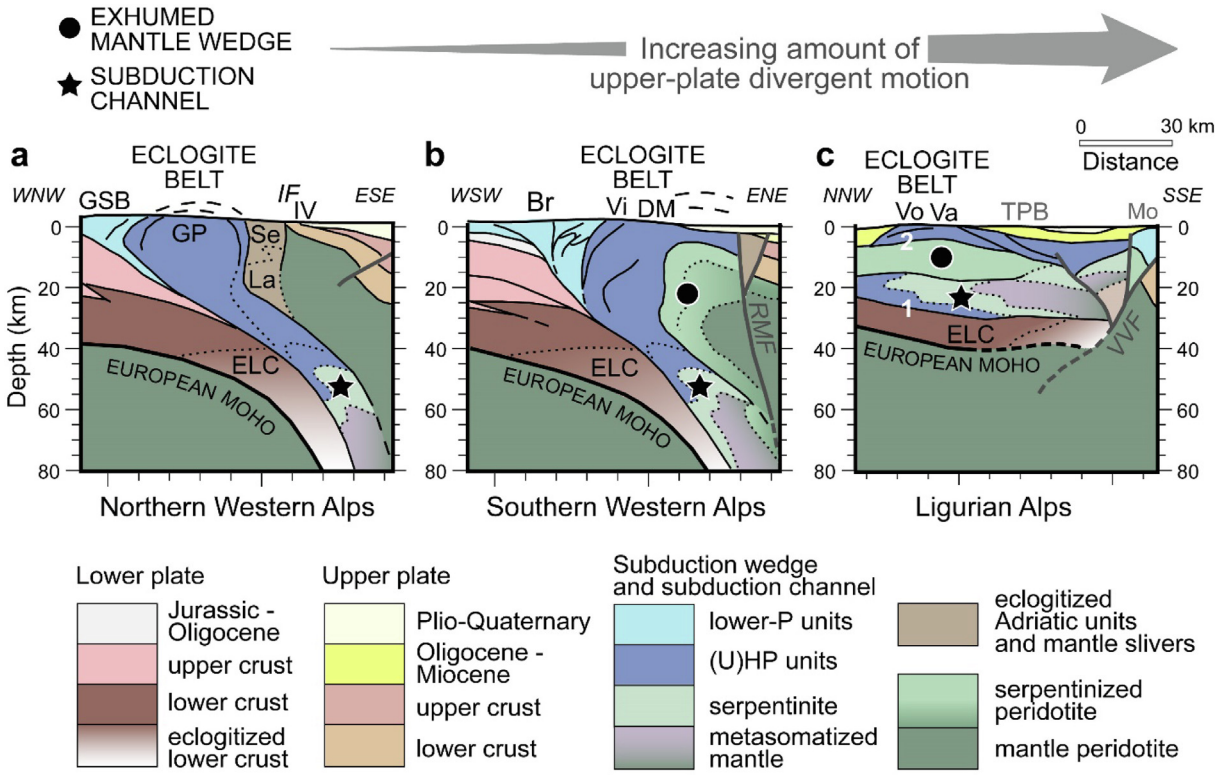

Fig. 7. Interpretive geologic cross sections showing the contrasting styles of exhumation of the mantle wedge and the subduction channel with increasing upper-plate divergence. a: CIFALPS2 ALP-S profile across the Gran Paradiso (GP) eclogitic dome. b: CIFALPS profile across the Dora-Maira (DM) eclogitic dome. c: CIFALPS2-Lig profile across the Valosio-Voltri (Va-Vo) eclogitic dome. Exhumation of the mantle wedge (black dots) beneath (U)HP rocks (dark blue) is exclusively observed for strong upper-plate divergence (b and c), as predicted by numerical models (e.g., Liao et al., 2018). Extreme upper-plate divergence (c) determines the uplift of the Moho together with the subduction channel (black star) and the overlying mantle wedge (black dot). The grey lines mark faults activated after (U)HP rock exhumation. 1 and 2 indicate interfaces marking a downward-increasing velocity change that are prone to be misinterpreted as a Moho. ELC=European lower crust. Other acronyms as in Fig. 1.

The creation of a flat subduction channel and an exhumed mantle wedge at shallow depth beneath the Ligurian Alps is a direct combination of the buoyancy of previously subducted rocks and the space created by the divergent motion of the upper plate that allows their exhumation (Fig. 5). For minor upper-plate divergence, the volume of rapidly exhumed buoyant crustal rocks previously stacked along the plate interface is sufficient to bridge the gap between the upper and lower plates after divergent motion (Fig. 7a). For major upper-plate divergent motion, however, the volume of subducted crustal rocks may be insufficient, and relatively buoyant serpentinized mantle rocks that originally lay deep above the lower plate may be exhumed beneath (U)HP continental crustal domes to bridge the residual gap (Fig. 7b, c). The potential involvement of the asthenospheric mantle is predicted only in the case of extreme divergent motion (Fig. 5).

5.2. High-pressure transformation of the European lower crust

Seismic velocities in the exhumed mantle wedge and subduction channel beneath the Ligurian Alps (Fig. 6) indicate that the original velocity structure acquired during subduction can be modified during the final stages of orogeny. A major impact of late collisional processes on seismic velocities was recently proposed by Sonnet et al. (2023) for the European lower crust along the CIFALPS profile, in disagreement with previous studies that have explained the reduction of the velocity contrast between the European lower crust and the underlying lithospheric mantle as an effect of the progressive eclogitization of a felsic-to-intermediate lower crust at depths >40 km during subduction (e.g., Zhao et al., 2015; Malusà et al., 2021; Paul et al., 2022). Sonnet et al. (2023) used an equilibrium-based modeling approach to calculate the relative abundance of mineral phases at lower crustal conditions and infer seismic velocities. They found that the Vs values observed in the European lower crust are consistent with felsic-to-intermediate rocks, either re-equilibrated under eclogitic facies conditions or under high-pressure granulitic facies conditions. However, they suggested that a high-pressure granulitic assemblage is more plausible, because the eclogitization of the European lower crust would have required preservation of a geothermal gradient of ~8°C/km during continental subduction, which they consider unlikely.

Their reasoning, however, is disproved by the pressure–tem perature-time paths of exhumed Alpine (U)HP continental rocks, which demonstrate that geothermal gradients in the Alpine subduction zone were still ~8°C/km during continental subduction (see Malusà et al., 2015, their Fig. 11). Therefore, the European lower crust located at depths >40 km necessarily underwent eclogitic facies metamorphism during the Alpine subduction cycle. However, since pressure–temperature-time paths also reveal a subsequent increase in paleogeothermal gradient after subduction (e.g., Malusà et al., 2006), a later overprint in the high-pressure granulite field cannot be excluded a priori. In any case, whether the subducted European lower crust is currently characterized by eclogitic facies assemblages (Zhao et al., 2015) or by high-pressure granulitic facies assemblages (Sonnet et al., 2023), we can conclude that the observed increase in its Vp and Vs values at ~40 km depth is necessarily related to mineral transformations under high-pressure conditions.

Further indications, however, are provided by local earthquake tomography and by the velocity structure of the European lower crust observed beneath the Ligurian Alps (Fig. 4f). Along the CIFALPS2-Lig profile, the Vp values between interfaces 1a and 5 progressively increase from ~7.0 km/s to ~7.5 km/s moving northward and at constant depth towards the Monferrato thrust front. Such polarity of northward-increasing Vp values is consistent with the polarity of Alpine subduction when considering the original dip angle of the European Moho, which subsequently became near-horizontal following upper-plate divergent motion. The velocity structure of the European lower crust is therefore supportive of a seismic velocity fingerprint largely acquired during subduction-related eclogitization rather than a late-stage granulite-facies overprint, which would produce constant velocities from south to north. This suggests that the eclogitized lower crust of the lower plate is less prone to metamorphic re-equilibration after subduction compared to the rocks of the overlying serpentinized mantle wedge and subduction channel (cf. Sect. 5.1).

5.3. Moho-like interfaces beneath the Ligurian Alps

As predicted by thermo-mechanical numerical models of (U)HP rock exhumation (Fig. 5) and described in Sect. 5.1, major upper-plate divergent motion may trigger exhumation of subduction-channel and mantle-wedge rocks at depth. As a result, a Moho-like interface may form beneath exhumed (U)HP domes, because crustal rocks end up being directly on top of exhumed mantle rocks, leading to a downward-increasing seismic-velocity change. A similar increase in seismic velocity with depth may also occur when rocks of a former subduction channel lay directly on top of an eclogitized lower crust belonging to the subducting lower plate. These interfaces should not be considered as a Moho, because they separate rocks that have been coupled together during subduction.

Abrupt vertical changes in seismic velocities interpreted as a Moho have long been recognized beneath the Ligurian Alps (e.g., Nicolich and Dal Piaz, 1992; Cassinis et al., 2005; Scafidi et al., 2009; Molli et al., 2010). However, the significance and dipping of such seismic velocity interfaces have been debated. For example, Nicolich and Dal Piaz (1992) proposed an Alpine Moho located at ~25 km depth for the Ligurian Alps, whereas Cassinis et al. (2005) suggested a south-dipping Ligurian transitional Moho in the 45–55 km depth range (Scafidi et al., 2009), and Molli et al. (2010) proposed a north-dipping Ligurian Moho from ~24 km depth in the Ligurian Alps to ~34 km depth in the Monferrato.

Our seismic tomography models are supportive of a Ligurian Moho exclusively developed offshore beneath the Ligurian Sea (7 in Fig. 4j). By contrast, the roots of the Ligurian Alps still preserve a north-dipping European Moho, progressively deepening from ~30 km depth near Genoa to ~40 km depth beneath the Voltri-Valosio (U)HP dome. The European Moho is not evident farther north, where it is likely parallel to the lower boundary of the resolved volume of the local earthquake tomography model (Fig. 4f and 7c). Along the CIFALPS2-Lig profile, the most evident interface marking a downward-increasing velocity change is represented by the lower boundary of the exhumed subduction channel (1 in Fig. 7c). This interface can be traced continuously both in the Vp (local-earthquake) and in the Vs (ambient-noise) tomography models (5 in Fig. 4f-j), from the Ligurian Sea in the south to the town of Asti in the north, where it is bounded by the Monferrato flower structure (MF in Fig. 4f). Because of the sharp transition from the low seismic velocities characterizing the low-temperature serpentinite of the exhumed subduction channel (Vp ~6.0 km/s; Vs ~3.0–3.1 km/s) to the much faster European lower crust underneath (Vp ~7.0–7.5 km/s), this interface could easily be, and indeed it was misinterpreted as a Moho, which is anyway ~10 km deeper and much less evident in seismic tomography. Notably, Molli et al. (2010) suggested a Ligurian Moho from ~24 km depth beneath the Ligurian Alps to ~34 km depth beneath Asti, right in the place and in the depth range where we have documented the lower boundary of the Alpine subduction channel.

Another interface marking a downward-increasing velocity change is located at 5–10 km depth beneath the Voltri-Valosio (U)HP dome (2 in Fig. 7c). This second interface marks the lower boundary of the dome, where continental crust rocks lay directly on top of partly serpentinized mantle-wedge rocks exhumed dur-

ing upper-plate divergent motion. Interface 2 has a smaller extension than interface 1 in map view and the velocity jump is less marked, which makes misinterpretations during Moho picking less likely. Salimbeni et al. (2021) used the term (proto)-continental Moho to indicate a similar interface between (U)HP continental crust units and mantle wedge rocks in the southern Western Alps (Solarino et al., 2018; Zhao et al., 2020). We emphasize that this interface, since it separates rocks that have been coupled during subduction, should not be considered a true Moho.

5.4. Distinguishing features of type-1 and type-2 Moho-like interfaces

Based on the evidence from the Ligurian Alps, two different types of Moho-like interfaces in a fossil subduction zone can therefore be distinguished: (i) type-1 interfaces that mark the base of a former subduction channel; and (ii) type-2 interfaces that mark the top of an exhumed mantle wedge. Both type-1 and type-2 interfaces are found beneath exhumed (U)HP rocks, which underlines the importance of a proper interpretation of seismic tomography models in (U)HP terranes. Distinguishing features of a type-1 Moho-like interface are the presence, above, of an additional interface with downward-decreasing velocity variation, marking the top of the subduction channel, and below of an interface with downward-increasing velocity variation, marking the Moho of the subducted lower plate. A distinguishing feature of a type-2 Moho-like interface is instead the presence, below the interface, of an additional interface with downward-decreasing velocity variation, marking the top of the subduction channel.

5.5. Comparison with a modern analog: Eastern Papua New Guinea

A re-evaluation of published seismic tomography models in the light of the results of the CIFALPS experiments reveals that Moho-like interfaces, such as those observed along the CIFALPS2-Lig profile, are not exclusive to the Western Alps, but are probably found in other subduction zones worldwide. This is for example the case of the (U)HP terrane of eastern Papua New Guinea (e.g., Jin et al., 2015; Abers et al., 2016), a geologically younger (i.e., late Miocene to present) analog for the Eocene Western Alps (Malusà and Garzanti, 2012; Liao et al., 2018) where rapid (U)HP rock exhumation is still active, and upper-plate divergent motion is replaced by ocean-continent collision in the Papuan mainland, the upper plate being oceanic (Baldwin et al., 2004, 2008, 2012; Webb et al., 2008; Wallace et al., 2014) (Fig. 8a). The D'Entrecasteaux Islands hosts the world's youngest (U)HP metamorphic rocks (Baldwin et al., 2004, 2008) and competing theories of plate divergence or diapiric upwelling have been suggested as driving their exhumation (Webb et al., 2008; Ellis et al., 2011; Little et al., 2011; Liao et al., 2018). These (U)HP rocks derive from northeastern Australian Cretaceous volcanoclastic sediments of the lower plate (e.g., Zirakparvar et al., 2013). No (U)HP metaophiolites are found on their top (Baldwin et al., 2012; Liao et al., 2018), possibly because the fast-spreading ridge off Australia, unlike the slow-spreading ridge of the Alpine Tethys, was not dominated by buoyant serpentinites (e.g., Guillot et al., 2015).

In eastern Papua New Guinea, tomography models reveal seismic velocities typical of mantle rocks at ~20 km depth beneath the (U)HP continental crust dome of Fergusson Island (F in Fig. 8-a-b) (Abers et al., 2016). The seismic dataset available to Abers et al. (2016), although not comparable with the CIFALPS dataset due to greater logistical difficulties and the location of the domes in the open sea, was recorded by 31 onshore broadband and 8 ocean bottom seismometers. Abers et al. (2016) jointly inverted Rayleigh wave dispersion curves with receiver functions waveforms for crustal velocity structure, and their results show similarities to the results shown in Figs. 4 and 7. As shown in Fig. 8b, they document crustal thinning and very low shear-wave velocities at all depths beneath the (U)HP domes of the D'Entrecasteaux Islands. In places, for example to the south of Fergusson Island, they detect multiple Moho-like discontinuities as observed beneath the Voltri-Valosio (U)HP dome, although available data do not allow discrimination between type-1 and type-2 Moho-like interfaces. Like in the CIFALPS2-Lig profile, Abers et al. (2016) found lower Vs values (~3.5 km/s) in the 20 km depth range beneath the (U)HP domes, and higher Vs values (~3.9 km/s) in the nearby regions of the Trobriand Platform and Goodenough Basin, in a similar fashion as in Fig. 4j. Shear-wave velocities taken either 5 km below the Moho or 5 km below the Moho-like interface underneath the exhumed (U)HP domes (Fig. 8b), show similar seismic velocity patterns as in the 20-km depth range, with lower Vs values beneath the domes (3.9–4.2 km/s) and higher Vs values on either side of the d'Entrecasteaux Islands (4.3–4.5 km/s). A similar situation is observed in the Alpine upper mantle, with Vs <4.5 km/s beneath the Voltri-Valosio and higher velocities (Vs >4.5 km/s) to the north, in the upper mantle beneath the Tertiary Piedmont Basin (Fig. 4j).

The seismic velocity structure beneath the D'Entrecasteaux (U)HP domes, which is often interpreted within a simple framework of continental rifting (Taylor et al., 1995; Abers et al., 2002; Ellis et al., 2011), is fully consistent with the velocity structure that is expected after subduction of the northern tip of the Australian plate and subsequent (U)HP rock exhumation (Baldwin et al., 2012; Webb et al., 2014). Remnants of a former subduction channel and exhumed mantle-wedge rocks may be still present beneath the D'Entrecasteaux (U)HP domes, as evidence of deep geological processes triggered by the localized divergence along the Australia-Pacific plate-boundary zone.

5.6. Long-term preservation of Moho-type interfaces: The Dabie Shan

The potential long-term preservation of the seismic velocity signature of Moho-type interfaces associated with a flat subduction channel and an exhumed mantle wedge following the exhumation of (U)HP rocks can be tested in pre-Cenozoic (U)HP terranes such as the Dabie Shan (Fig. 8c, d), where continental eclogites were formed in the Triassic by subduction of the Yangtze Craton beneath the North China Craton (Hacker et al., 2004; Liou et al., 2009). Exhumation was completed in the Jurassic (Li et al., 2010; Baldwin et al., 2019). Like in the Western Alps and in eastern Papua New Guinea, the role of erosion in the Dabie Shan was negligible during the main (U)HP rock exhumation stage (Malusà et al., 2011). Seismic reflection and receiver function data (Wang et al., 2000; Xue-Cheng et al., 2003; Dong et al., 2008; Zheng et al., 2012) reveal that the Moho beneath the Dabie Shan dips northward, consistent with subduction of the Yangtze Craton. The discontinuous velocity interfaces imaged by receiver function beneath the southern North China Craton have been interpreted as the remnants of a flat subduction channel (Zheng et al., 2012). However, deep-reflection and shallow-tomography studies exclude the presence of a deep crustal root inherited from continental subduction (Schmid et al., 2001). As a result, the Dabie Shan is classically interpreted as a crustal-scale dome formed during post-collisional uplift by core-complex–type exhumation of the lower crust, tectonically unrelated to the early stages of (U)HP rock exhumation (Hacker et al., 2000; Xue-Cheng et al., 2003).

Beneath the South and Central Dabie, a high-velocity dome-shaped anomaly has been imaged by ambient-noise tomography at depths as shallow as ~12 km in the middle crust (Luo et al., 2012). The formation of this high velocity dome has been interpreted in terms of post-collisional delamination of the lithosphere and subsequent magmatism (Li et al., 2005), with the high velocities marking intrusive and underplated igneous rocks generated at the base of a collision-thickened orogen (Zhao and Zheng, 2009). At

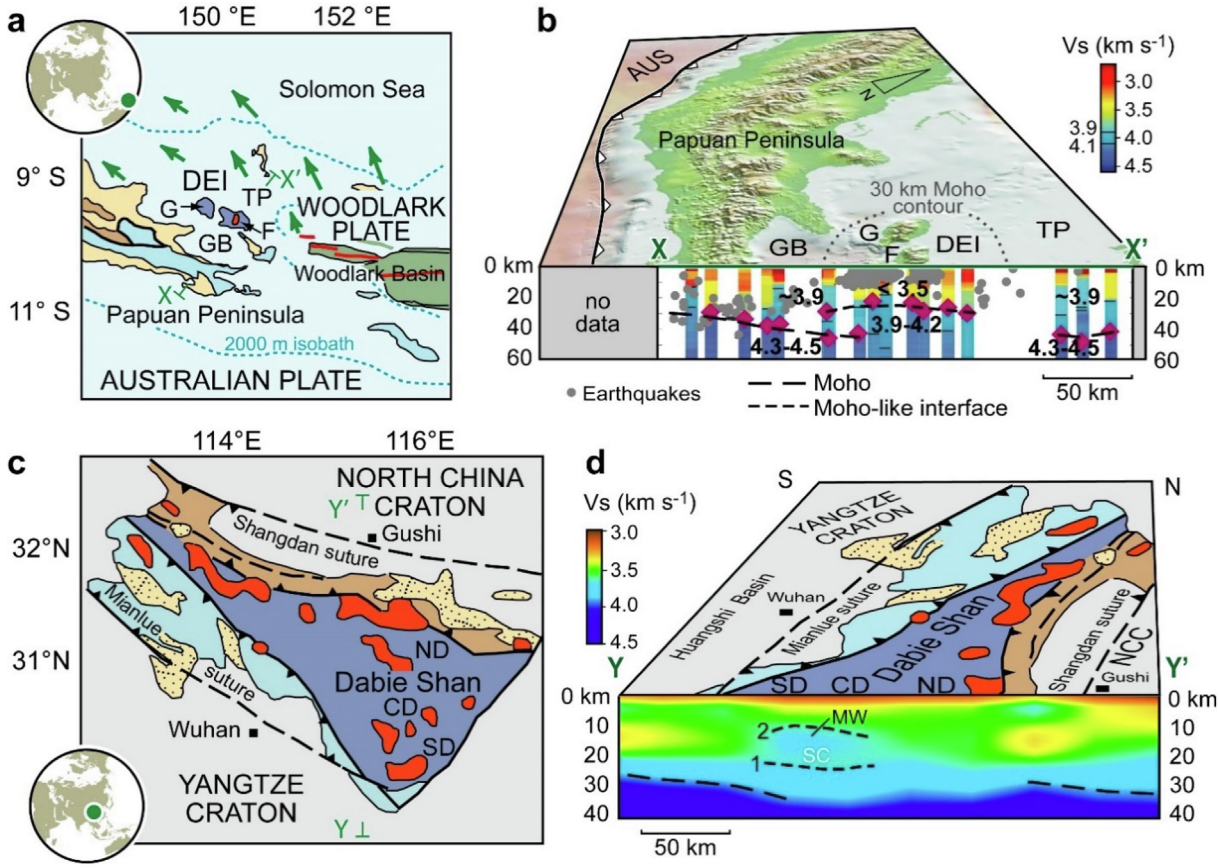

Fig. 8. Comparison with other (U)HP terranes. a: Tectonic sketch map of the (U)HP terrane of eastern Papua New Guinea (after Baldwin et al., 2008), which is considered as a modern analog of the Western Alps in the Late Eocene. Acronyms: DEI, D'Entrecasteaux Islands; F, Fergusson Island; G, Goodenough Island; GB, Goodenough Basin; TP, Trobriand platform. X-X' indicates the location of the cross section shown in frame b. b: Vs structure beneath the D'Entrecasteaux Islands (DEI), based on joint inversion of receiver function waveforms with Rayleigh wave dispersion curves (after Abers et al., 2016). Dashed black lines indicate the Moho of the Australian (AUS) lower plate, the Moho of the Woodlark upper plate, and a Moho-like interface beneath the DEI (U)HP domes. Magenta diamonds = maximum-likelihood interfaces identified as Moho by Abers et al. (2016). Numbers in bold = Vs in km/s. c: Tectonic sketch map of the Dabie Shan (U)HP terrane (after Li et al., 2010). Acronyms: CD=Central Dabie; ND=North Dabie; SD=South Dabie. Y-Y' indicates the location of the cross section shown in frame d. d: Reinterpreted Vs structure beneath the Dabie Shan based on ambient-noise tomography (after Luo et al., 2012). 1 and 2 indicate Moho-like interfaces marking the base of a former subduction channel (SC) and the top of an exhumed mantle wedge (MW); NCC=North China Craton. Note that both in eastern Papua New Guinea and the Dabie Shan, Moho-like interfaces are found in the same position and depth range as in the CIFALPS2-Lig profile of the Western Alps. Color codes: dark blue = (U)HP rocks; light blue = lower-pressure units; brown = older orogenic wedges or magmatic arcs; yellow = post-orogenic sedimentary rocks; orange = Cenozoic plutons (in a) or post-Jurassic granites (in c, d).

the base of the high velocity dome, ambient-noise tomography reveals a low-Vs near-horizontal layer at ~20–25 km depth (Luo et al., 2012).

A comparison of Fig. 8d with the CIFALPS2-Lig profile, however, reveals several analogies with the seismic velocity structure of the fossil subduction zone of the Western Alps. This suggests that the deep tectonic structure beneath the South and Central Dabie may be partly inherited from the (U)HP exhumation stage. Fig. 8d shows that the deep structure of the Dabie Shan, as the Ligurian Alps, lacks a deep crustal root, and may include an exhumed mantle wedge as shallow as ~12 km (MW in Fig. 8d) beneath the (U)HP crustal rocks of the South and Central Dabie, and the remnants of a near-horizontal subduction channel (SC in Fig. 8d) at depths around 20–25 km, still preserved on top of the subducted lower crust and lithospheric mantle of the Yangtze Craton. The north-dipping Moho of the lower plate can be traced from 30 to 35 km depth beneath the Huangshi Basin and is replaced northwards by two Moho-like interfaces: a type-1 interface marking the base of the former subduction channel (1 in Fig. 8d) and a type-2 interface marking the top of the exhumed mantle wedge (2 in Fig. 8d). The Moho of the North China Craton lies farther north at a depth of 30–35 km beneath the Shangdan suture (Fig. 8d). The consistency between the Alpine and Dabie Shan seismic velocity structure suggests that the results of the CIFALPS experiments can be used as a reference case for the interpretation of the deep tectonic structure not only of other Cenozoic (U)HP terranes, but also much older ones.

6. Conclusion

The results of the CIFALPS seismic experiments reveal contrasting styles of exhumation of subduction-channel and mantle-wedge rocks triggered by upper-plate divergent motion after continental subduction. For low amounts of upper-plate divergence (e.g., the northern Western Alps), a thickened subduction channel can be detected, but no exhumed mantle wedge is found beneath the dome of exhumed continental (U)HP rocks. For intermediate divergence (e.g., the southern Western Alps), an exhumed mantle wedge is detected at depths from ~10 km to >30 km in between the (U)HP tectonic dome and the serpentinized subduction channel. For higher divergence (e.g., the Ligurian Alps), an exhumed mantle wedge and a former subduction channel are recognized at much shallower levels beneath the tectonic dome of exhumed (U)HP rocks, and above a shallow-dipping lower-plate Moho. In this case, the lower boundary of the exhumed subduction channel is invari-

ably the most evident interface marking a downward-increasing velocity change, forming a Moho-like interface that may be easily misinterpreted as a true Moho. Similar Moho-like interfaces are found beneath the exhumed (U)HP tectonic domes of eastern Papua New Guinea and the Dabie Shan, which suggests that the results of the CIFALPS passive seismic experiments may be used as a reference case for the interpretation of other (U)HP terranes worldwide.

CRediT authorship contribution statement

Stefano Solarino: Writing – review & editing, Validation, Software, Resources, Project administration, Methodology, Investigation, Formal analysis, Data curation. **Marco G. Malusà:** Conceptualization, validation, Investigation, Writing – original draft, Visualization. **Elena Eva:** Writing – review & editing, Investigation, Formal analysis, Data curation. **Anne Paul:** Writing – review & editing, Validation, Resources, Project administration, Methodology, Investigation, Formal analysis, Data curation. **Stéphane Guillot:** Writing – review & editing, Conceptualization. **Silvia Pondrelli:** Investigation, Data curation. **Simone Salimbeni:** Data curation. **Liang Zhao:** Supervision, Resources, Project administration, Funding acquisition, Conceptualization.

Declaration of competing interest

The authors declare that they have no known competing financial interests or personal relationships that could have appeared to influence the work reported in this paper.

Acknowledgments

This project is funded by the National Natural Science Foundation of China (Grant 41625016, 41888101) and the National Key R&D Program of China (Grant No.2017YFC0601201).

Appendix A. Supplementary material

Supplementary data to this article can be found online at https://doi.org/10.1016/j.gr.2024.08.016.

References

Abers, G.A., Ferris, A., Craig, M., Davies, H., Lerner-Lam, A.L., Mutter, J.C., Taylor, B., 2002. Mantle compensation of active metamorphic core complexes at Woodlark rift in Papua New Guinea. Nature 418 (6900), 862–865.

Abers, G.A., Eilon, Z., Gaherty, J.B., Jin, G., Kim, Y.H., Obrebski, M., Dieck, C., 2016. Southeast Papuan crustal tectonics: Imaging extension and buoyancy of an active rift. J. Geophys. Res. Solid Earth 121 (2), 951–971.

Baldwin, S.L., Monteleone, B.D., Webb, L.E., Fitzgerald, P.G., Grove, M., June Hill, E., 2004. Pliocene eclogite exhumation at plate tectonic rates in eastern Papua New Guinea. Nature 431 (7006), 263–267.

Baldwin, S.L., Webb, L.E., Monteleone, B.D., 2008. Late Miocene coesite-eclogite exhumed in the Woodlark Rift. Geology 36 (9), 735–738.

Baldwin, S.L., Fitzgerald, P.G., Webb, L.E., 2012. Tectonics of the New Guinea region. Annu. Rev. Earth Planet. Sci. 40, 495–520.

Baldwin, S.L., Fitzgerald, P.G., Malusà, M.G., 2019. Crustal exhumation of plutonic and metamorphic rocks: constraints from fission-track thermochronology. Fission-Track Thermochronology and Its Application to Geology, 235–257.

Berra, F., Galli, M.T., Reghellin, F., Torricelli, S., Fantoni, R., 2009. Stratigraphic evolution of the Triassic-Jurassic succession in the Western Southern Alps (Italy): the record of the two-stage rifting on the distal passive margin of Adria. Basin Res. 21 (3), 335–353.

Cassano, E., Anelli, L., Fichera, R., Cappelli, V. (1986). Pianura Padana, interpretazione integrata di dati geofisici e geologici. AGIP Servizi Centrali per l'Esplorazione, Metodologie e Appl. Geofisiche, Milano.

Cassinis, R., Scarascia, S., & Lozej, A. (2005). Review of Seismic Wide-Angle Reflection-Refraction (WARR). Results in the Italian Region (1956–1987). In: Finetti, I.R. (Ed.), Crop Project, Deep Seismic Exploration of the Central Mediterranean and Italy. Atlas in Geophysics. Elsevier, pp. 31–55.

Chen, Y.X., Zhou, K., He, Q., Zheng, Y.F., Schertl, H.P., Chen, K., 2023. First finding of continental deep subduction in the Sesia Zone of the Western Alps and implications for subduction dynamics. Natl. Sci. Rev. 10(5), nwad023.

Chopin, C., 1984. Coesite and pure pyrope in high-grade blueschists of the Western Alps: a first record and some consequences. Contrib. Miner. Petrol. 86, 107–118.

Dong, S.W., Li, Q.S., Gao, R., Liu, F.T., Xu, P.F., Liu, X.C., Guan, Y., 2008. Moho-mapping in the Dabie ultrahigh-pressure collisional orogen, central China. Am. J. Sci. 308 (4), 517–528.

Dumont, T., Schwartz, S., Guillot, S., Malusà, M., Jouvent, M., Monié, P., Verly, A., 2022. Cross-propagation of the western Alpine orogen from early to late deformation stages: Evidence from the Internal Zones and implications for restoration. Earth Sci. Rev. 104106.

Eberhart-Phillips, D., 1990. Three-dimensional P and S velocity structure in the Coalinga region, California. J. Geophys. Res. Solid Earth 95 (B10), 15343–15363.

Ellis, S.M., Little, T.A., Wallace, L.M., Hacker, B.R., Buiter, S.J.H., 2011. Feedback between rifting and diapirism can exhume ultrahigh-pressure rocks. Earth Planet. Sci. Lett. 311 (3–4), 427–438.

Eva, E., Malusà, M.G., Solarino, S., 2015. A seismotectonic picture of the inner southern Western Alps based on the analysis of anomalously deep earthquakes. Tectonophysics 661, 190–199.

Eva, E., Malusà, M.G., Solarino, S., 2020. Seismotectonics at the transition between opposite-dipping slabs (western Alpine region). Tectonics 39 (9). e2020TC006086.

Eva, E., Malusà, M.G., Solarino, S., 2023. The 2021–2022 Genoa seismic sequences reveal distributed strike-slip deformation in the Alps-Apennines transition zone. NW Italy. Tectonophysics 868, 230101.

Ghignone, S., Scaramuzzo, E., Bruno, M., Livio, F.A., 2023. A new UHP unit in the Western Alps: First occurrence of coesite from the Monviso Massif (Italy). Am. Mineral. 108 (7), 1368–1375.

Guillot, S., Schwartz, S., Reynard, B., Agard, P., Prigent, C., 2015. Tectonic significance of serpentinites. Tectonophysics 646, 1–19.

Hacker, B.R., Ratschbacher, L., Webb, L., McWilliams, M.O., Ireland, T., Calvert, A., Chateigner, D., 2000. Exhumation of ultrahigh-pressure continental crust in east central China: Late Triassic-Early Jurassic tectonic unroofing. J. Geophys. Res. Solid Earth 105 (B6), 13339–13364.

Hacker, B.R., Ratschbacher, L., Liou, J.G., 2004. Subduction, collision and exhumation in the ultrahigh-pressure Qinling-Dabie orogen. Geol. Soc. Lond. Spec. Publ. 226 (1), 157–175.

Handy, M.R., Schmid, S.M., Bousquet, R., Kissling, E., Bernoulli, D., 2010. Reconciling plate-tectonic reconstructions of Alpine Tethys with the geological–geophysical record of spreading and subduction in the Alps. Earth Sci. Rev. 102 (3–4), 121–158.

Haslinger, F., Kissling, E., 2001. Investigating effects of 3-D ray tracing methods in local earthquake tomography. Phys. Earth Planet. In. 123 (2–4), 103–114.

Hetényi, G., Molinari, I., Clinton, J., Bokelmann, G., Bondár, I., Crawford, W. C., ... & AlpArray Working Group. (2018). The AlpArray seismic network: a large-scale European experiment to image the Alpine Orogen. Surveys in geophysics, 39, 1009-1033.

Jin, G., Gaherty, J.B., Abers, G.A., Kim, Y., Eilon, Z., Buck, W.R., 2015. Crust and upper mantle structure associated with extension in the Woodlark Rift, Papua New Guinea from Rayleigh-wave tomography. Geochem. Geophys. Geosyst. 16 (11), 3808–3824.

Kissling, E., 1988. Geotomography with local earthquake data. Rev. Geophys. 26 (4), 659–698.

Langston, C.A., 1979. Structure under Mount Rainier, Washington, inferred from teleseismic body waves. J. Geophys. Res. Solid Earth 84 (B9), 4749–4762.

Li, S., Kusky, T.M., Zhao, G., Liu, X., Zhang, G., Kopp, H., Wang, L., 2010. Two-stage Triassic exhumation of HP–UHP terranes in the western Dabie orogen of China: constraints from structural geology. Tectonophysics 490 (3–4), 267–293.

Li, S.G., Li, Q.L., Hou, Z.H., Yang, W., Wang, Y., 2005. Cooling history and exhumation mechanism of the ultrahigh-pressure metamorphic rocks in the Dabie mountains, central China. Acta Petrol. Sin. 21 (4), 1117–1124.

Liao, J., Malusà, M.G., Zhao, L., Baldwin, S.L., Fitzgerald, P.G., Gerya, T., 2018. Divergent plate motion drives rapid exhumation of (ultra) high pressure rocks. Earth Planet. Sci. Lett. 491, 67–80.

Liou, J.G., Ernst, W.G., Zhang, R.Y., Tsujimori, T., Jahn, B.M., 2009. Ultrahigh-pressure minerals and metamorphic terranes–the view from China. J. Asian Earth Sci. 35 (3–4), 199–231.

Little, T.A., Hacker, B.R., Gordon, S.M., Baldwin, S.L., Fitzgerald, P.G., Ellis, S., Korchinski, M., 2011. Diapiric exhumation of Earth's youngest (UHP) eclogites in the gneiss domes of the D'Entrecasteaux Islands. Papua New Guinea. Tectonophysics 510 (1–2), 39–68.

Luo, Y., Xu, Y., Yang, Y., 2012. Crustal structure beneath the Dabie orogenic belt from ambient noise tomography. Earth and Planetary Science Letters 313, 12–22.

Maffione, M., Speranza, F., Faccenna, C., Cascella, A., Vignaroli, G., Sagnotti, L., 2008. A synchronous Alpine and Corsica-Sardinia rotation. J. Geophys. Res. Solid Earth 113 (B3).

Malusà, M.G., Balestrieri, M.L., 2012. Burial and exhumation across the Alps-Apennines junction zone constrained by fission-track analysis on modern river sands. Terra Nova 24 (3), 221–226.

Malusà, M.G., Faccenna, C., Baldwin, S.L., Fitzgerald, P.G., Rossetti, F., Balestrieri, M. L., Danišík, M., Ellero, A., Ottria, G., Piromallo, C., 2015. Contrasting styles of (U) HP rock exhumation along the Cenozoic Adria-Europe plate boundary (Western Alps, Calabria, Corsica). Geochem. Geophys. Geosyst. 16 (6), 1786–1824.

Malusà, M.G., Anfinson, O.A., Dafov, L.N., Stockli, D.F., 2016. Tracking Adria indentation beneath the Alps by detrital zircon U-Pb geochronology:

Implications for the Oligocene-Miocene dynamics of the Adriatic microplate. Geology 44 (2), 155–158.
Malusà, M.G., Garzanti, E., 2012. Actualistic snapshot of the early Oligocene Alps: the Alps-Apennines knot disentangled. Terra Nova 24 (1), 1–6.
Malusà, M.G., Polino, R., Martin, S., 2005. The Gran San Bernardo nappe in the Aosta valley (western Alps): a composite stack of distinct continental crust units. Bulletin De La Société Géologique De France 176 (5), 417–431.
Malusà, M.G., Philippot, P., Zattin, M., Martin, S., 2006. Late stages of exhumation constrained by structural, fluid inclusion and fission track analyses (Sesia–Lanzo unit, Western European Alps). Earth Planet. Sci. Lett. 243 (3–4), 565–580.
Malusà, M.G., Faccenna, C., Garzanti, E., Polino, R., 2011. Divergence in subduction zones and exhumation of high pressure rocks (Eocene Western Alps). Earth Planet. Sci. Lett. 310 (1–2), 21–32.
Malusà, M.G., Zhao, L., Eva, E., Solarino, S., Paul, A., Guillot, S., Zhu, R., 2017. Earthquakes in the western Alpine mantle wedge. Gondw. Res. 44, 89–95.
Malusà, M.G., Guillot, S., Zhao, L., Paul, A., Solarino, S., Dumont, T., Schwartz, S., Aubert, C., Baccheschi, P., Eva, E., Lu, Y., Lyu, C., Pondrelli, S., Salimbeni, S., Sun, W., Yuan, H., 2021. The deep structure of the Alps based on the CIFALPS seismic experiment: A synthesis. Geochem. Geophys. Geosyst. 22 (3). e2020GC009466.
Manzotti, P., Schiavi, F., Nosenzo, F., Pitra, P., Ballèvre, M., 2022. A journey towards the forbidden zone: a new, cold, UHP unit in the Dora-Maira Massif (Western Alps). Contrib. Miner. Petrol. 177 (6), 59.
Menichelli, I., De Gori, P., Lucente, F.P., Improta, L., Chiarabba, C., 2023. Lithosphere Structure, Processes, and Physical State of the Alpine-Apennine System. J. Geophys. Res. Solid Earth 128 (4). e2023JB026411.
Millet, F., Bodin, T., Rondenay, S., 2019. Multimode 3-D Kirchhoff migration of receiver functions at continental scale. J. Geophys. Res. Solid Earth 124 (8), 8953–8980.
Molli, G., Crispini, L., Malusà, M., Mosca, P., Piana, F., Federico, L., 2010. Geology of the Western Alps-Northern Apennine junction area: a regional review. Eds Marco Beltrando, Angelo Peccerillo, Massimo Mattei, Sandro Conticelli, and Carlo Doglioni Journal of the Virtual Explorer 36 (3).
Nicolich, R., & Dal Piaz, G.V. (1992). Moho isobaths. Structural Model of Italy Scale 1:500.000. Quaderni de "La Ricerca Scientifica", 114 (3), CNR.
Nouibat, A., Brossier, R., Stehly, L., Cao, J., Paul, A., & Cifalps Team and AlpArray Working Group. (2023). Ambient-Noise Wave-Equation Tomography of the Alps and Ligurian-Provence Basin. Journal of Geophysical Research: Solid Earth, 128(10), e2023JB026776.
Nouibat, A., Stehly, L., Paul, A., Schwartz, S., Bodin, T., Dumont, T., Rolland, Y., Brossier, R., Cifalps Team & AlpArray Working Group, 2022. Lithospheric transdimensional ambient-noise tomography of W-Europe: implications for crustal-scale geometry of the W-Alps. Geophys. J. Int. 229 (2), 862–879.
Paul, A., Malusà, M.G., Solarino, S., Salimbeni, S., Eva, E., Nouibat, A., Zhao, L., 2022. Along-strike variations in the fossil subduction zone of the Western Alps revealed by the CIFALPS seismic experiments and their implications for exhumation of (ultra-) high-pressure rocks. Earth Planet. Sci. Lett. 598, 117843.
Rondenay, S., 2009. Upper mantle imaging with array recordings of converted and scattered teleseismic waves. Surv. Geophys. 30 (4), 377–405.
Rubatto, D., Hermann, J., 2001. Exhumation as fast as subduction? Geology 29 (1), 3–6.
Rubatto, D., Muentener, O., Barnhoorn, A., Gregory, C., 2008. Dissolution-reprecipitation of zircon at low-temperature, high-pressure conditions (Lanzo Massif, Italy). Am. Mineral. 93 (10), 1519–1529.
Salimbeni, S., Agostinetti, N. P., Pondrelli, S., & CIFALPS Working Group. (2021). Insights into the origin and deformation style of the continental Moho: A case-study from the Western Alps (Italy). Journal of Geophysical Research: Solid Earth, 126(6), e2020JB021319.
Scafidi, D., Solarino, S., Eva, C., 2009. P wave seismic velocity and Vp/Vs ratio beneath the Italian peninsula from local earthquake tomography. Tectonophysics 465 (1–4), 1–23.
Schmid, R., Ryberg, T., Ratschbacher, L., Schulze, A., Franz, L., Oberhänsli, R., Dong, S., 2001. Crustal structure of the eastern Dabie Shan interpreted from deep reflection and shallow tomographic data. Tectonophysics 333 (3–4), 347–359.
Schmidt, M.W., Vielzeuf, D., Auzanneau, E., 2004. Melting and dissolution of subducting crust at high pressures: the key role of white mica. Earth Planet. Sci. Lett. 228 (1–2), 65–84.
Solarino, S., Malusà, M.G., Eva, E., Guillot, S., Paul, A., Schwartz, S., Zhu, R., 2018. Mantle wedge exhumation beneath the Dora-Maira (U) HP dome unravelled by local earthquake tomography (Western Alps). Lithos 296, 623–636.
Solarino, S. (2024). Temporary seismic stations boost tomography capability to look into the earth. Case studies in the Northwestern Alps, Italy. Canadian Association of Exploration Geophysicists. https://cseg.ca/temporary-seismic-stations-boost-tomography-capability-to-look-into-the-earth-case-studies-in-the-northwestern-alps-italy/.
Sonnet, M., Labrousse, L., Bascou, J., Plunder, A., Nouibat, A., Paul, A., 2023. Assessing Chemical and Mineralogical Properties of the Alpine Slab Based on Field Analogs and Ambient Noise Tomography. Geochem. Geophys. Geosyst. https://doi.org/10.1029/2022GC010784.
Starr, P.G., Broadwell, K.S., Dragovic, B., Scambelluri, M., Haws, A.A., Caddick, M.J., Baxter, E.F., 2020. The subduction and exhumation history of the Voltri Ophiolite, Italy: Evaluating exhumation mechanisms for high-pressure metamorphic massifs. Lithos 376, 105767.
Taylor, B., Goodliffe, A., Martinez, F., Hey, R., 1995. Continental rifting and initial sea-floor spreading in the Woodlark Basin. Nature 374 (6522), 534–537.
Thurber, C.H., 1983. Earthquake locations and three-dimensional crustal structure in the Coyote Lake area, central California. J. Geophys. Res. Solid Earth 88 (B10), 8226–8236.
Virieux, J., Paul, A., Langlais, M., Janex, G., Gueguen, P., Helmstetter, A., Stehly, L., 2024. Assessing the reliability of local earthquake tomography for crustal imaging: 30 yr of records in the Western Alps as a case study. Geophys. J. Int. 236 (1), 99–118.
Wallace, L.M., Ellis, S., Little, T., Tregoning, P., Palmer, N., Rosa, R., Kwazi, J., 2014. Continental breakup and UHP rock exhumation in action: GPS results from the W oodlark Rift, Papua New Guinea. Geochem. Geophys. Geosyst. 15 (11), 4267–4290.
Wang, C.Y., Zeng, R.S., Mooney, W.D., Hacker, B.R., 2000. A crustal model of the ultrahigh-pressure Dabie Shan orogenic belt, China, derived from deep seismic refraction profiling. J. Geophys. Res. Solid Earth 105 (B5), 10857–10869.
Webb, L.E., Baldwin, S.L., Little, T.A., Fitzgerald, P.G., 2008. Can microplate rotation drive subduction inversion? Geology 36 (10), 823–826.
Webb, L.E., Baldwin, S.L., Fitzgerald, P.G., 2014. The Early-Middle Miocene subduction complex of the Louisiade Archipelago, southern margin of the Woodlark Rift. Geochem. Geophys. Geosyst. 15 (10), 4024–4046.
Xue-Cheng, Y., Klemperer, S.L., Wen-Bang, T., Lai-Xiang, L., Chetwin, E., 2003. Crustal structure and exhumation of the Dabie Shan ultrahigh-pressure orogen, eastern China, from seismic reflection profiling. Geology 31 (5), 435–438.
Zahorec, P., Papčo, J., Pašteka, R., Bielik, M., Bonvalot, S., Braitenberg, C., et al., 2021. The first pan-Alpine surface-gravity database, a modern compilation that crosses frontiers. Earth Syst. Sci. Data 13 (5), 2165–2209.
Zhao, L., M.G. Malusà, H. Yuan, A. Paul, S. Guillot, Y. Lu, S. Solarino, E. Eva, G. Lu, T. Bodin, Cifalps Group, AlpArray Working Group, 2020. Evidence for a serpentinized plate interface favouring continental subduction. Nature communications, 11(1), 1-8.
Zhao, L., Paul, A., Guillot, S., Solarino, S., Malusà, M.G., Zheng, T.Y., Aubert, C., Salimbeni, S., Dumont, T., Schwartz, S., Zhu, R.X., Wang, Q.C., 2015. First seismic evidence for continental subduction beneath the Western Alps. Geology 43 (9), 815–818.
Zhao, L., Paul, A., Solarino, S., Resif,, 2016. Seismic network YP: CIFALPS temporary experiment (China-Italy-France Alps seismic transect). RESIF - Réseau Sismologique et Géodésique Français.
Zhao, L., Paul, A., Solarino, S., Resif,, 2018. Seismic network XT: CIFALPS2 temporary experiment (China-Italy-France Alps seismic transect #2). RESIF - Réseau Sismologique et Géodésique Français.
Zhao, Z., Zheng, Y., 2009. Remelting of subducted continental lithosphere: Petrogenesis of Mesozoic magmatic rocks in the Dabie-Sulu orogenic belt. Sci China Ser D Earth Sci 52 (9), 1295–1318.
Zheng, T., Zhu, R., Zhao, L., Ai, Y., 2012. Intralithospheric mantle structures recorded continental subduction. J. Geophys. Res. Solid Earth 117 (B3).
Zirakparvar, N.A., Baldwin, S.L., Vervoort, J.D., 2013. The origin and geochemical evolution of the Woodlark Rift of Papua New Guinea. Gondw. Res. 23 (3), 931–943.